Cyclin D1 Overexpression Induces Replication Stress and Microhomology-Mediated End-Joining Dependence in Mantle Cell Lymphoma

Jithma Prasad Abeykoon[1,2#], Shuhei Asada[2#], Guangli Zhu[2,3#], Yuna Hirohashi[2], Lisa Moreau[2], Divya Iyer[2,4], Sirisha Mukkavalli[2], Kalindi Parmar[2], Gabriella Zambrano[2], Lige Jiang[1,5], Dongni Yi[1], Michelle Manske[1], Kimberly Gwin[1], Rebecca King[6], James R Cerhan[7], Xiaosheng Wu[1], Zhenkun Lou[8], Geoffrey I Shapiro[9], Thomas Witzig[1] and Alan D'Andrea[2]

1. Division of Hematology, Department of Internal Medicine, Mayo Clinic, MN, USA
2. Department of Radiation Oncology, Dana-Farber Cancer Institute, Boston, MA, USA
3. Department of Radiation Oncology, The First Affiliated Hospital of Sun Yat-sen University, Guangzhou 510080, PR China
4. Bayer Pharmaceuticals, Cambridge, MA
5. Nova Southeastern University, Dr. Kiran C Patel College of Osteopathic Medicine, FL, USA
6. Department of Pathology, Mayo Clinic, MN, USA
7. Department of Quantitative Health Sciences, Mayo Clinic, MN
8. Department of Oncology, Mayo Clinic, MN, USA
9. Department of Medical Oncology, Dana-Farber Cancer Institute, Boston, MA, USA

# equal contribution

Corresponding Author
Alan D'Andrea, M.D.
Department of Radiation Oncology,
Dana-Farber Cancer Institute,
Boston, MA, USA.

Kew words: DNA damage repair, oncogene, treatments, alternative end-joining, theta-mediated end-joining

Short title: Targeting MMEJ in CCND1 overexpressed cancers

Conflict of Interests

Dr. Shapiro has research funding from Merck KGaA/EMD-Serono, Tango Therapeutics, Bristol Myers Squibb, Merck & Co., Artios, Lilly and Pfizer. He has served on advisory boards for Merck KGaA/EMD-Serono, Circle Pharmaceuticals, Concarlo Therapeutics, Schrodinger, FoRx Therapeutics and Xinthera. He holds patents entitled, “Dosage regimen for sapacitabine and seliciclib,” and “Compositions and Methods for Predicting Response and Resistance to CDK4/6 inhibition.” Dr. Witzig gets clinical trials research support to Mayo Clinic from Acerta, Incyte, Kura Oncology and Karyopharm. Dr. Witzig serves in the advisor board and get personally compensated in AbbVie, and Global commercial Epcoritamab Advisory Board. The rest of the authors have declared no conflict of interest exists.

Abstract

Oncogene expression can cause replication stress (RS), leading to DNA double-strand breaks (DSB) that require repair through pathways such as homologous recombination, non-homologous end-joining, and microhomology-mediated end-joining (MMEJ). Cyclin D1 (encoded by *CCND1*) is a well-known oncoprotein overexpressed in cancer; however, its role in RS is unknown. Using mantle cell lymphoma (MCL) as a naturally occurring model of cyclin D1 overexpression, we examined its impact on RS and DSB-repair mechanisms. Cyclin D1 overexpression elevated RS, increased DNA damage, especially during mitosis, and caused specific upregulation of MMEJ. Furthermore, cyclin D1 activates the polymerase theta (*POLQ*) transcription by binding its promoter loci, driving POLΘ-mediated MMEJ that is essential to withstand cyclin D1-induced RS. Moreover, concurrent ATM deficiency further intensifies RS, enhances *POLQ* expression and heightens reliance on MMEJ mediated DNA damage repair. Consequently, inhibition of POLΘ in cyclin D1-overexpressed settings further exacerbates RS, causing single-strand DNA gap accumulations and chromosomal instability, ultimately leading to apoptosis, an effect amplified in ATM-deficient cells. Targeting MMEJ via POLΘ inhibition is, therefore, an effective strategy in the context of cyclin D1 overexpression and ATM deficiency and may provide a unique therapeutic approach for treating MCL and other malignancies characterized by similar alterations.

Introduction

Despite the inherent accuracy of DNA replication, various exogenous and endogenous stresses experienced by cells, collectively termed “replication stress (RS),” challenge the fidelity of this highly sophisticated machinery. RS results in replication fork slowing, increased single-stranded DNA gaps, reduced replication fidelity, and the generation of double-strand DNA breaks (DSBs) (1-3). DSBs can be lethal if not repaired by pathways such as homologous recombination (HR), non-homologous end joining (NHEJ), or microhomology-mediated end-joining (MMEJ) (4). These DSB repair pathways are highly cell cycle regulated and occur during the S/G_2-phases, G_1-phase, or mitosis, respectively (5, 6).

Oncogene overexpression such as *c-Myc*(7), *K-RAS*(8) and *BCL-2*(9) among many others, with its resultant high proliferation rate, is a major source of RS. Heightened RS is proportional to the generation of DSBs, which in turn can overwhelm the DSB repair pathways and produce a high DSB burden (3). Furthermore, oncogene expression can also perturb cell cycle checkpoints, causing unrepaired DSB to traverse the cell cycle without activation of cell cycle arrest (10-15). Therefore, unrepaired DSBs can accumulate in mitosis, a time when the HR and NHEJ pathways are inactive (16, 17). Consequently, cancer cells driven by oncogene-induced proliferation rely heavily on the MMEJ pathway for DSB repair.

Cyclin D1 (encoded by *CCND1*) is frequently overexpressed in cancers by a variety of mechanisms (18). In addition to gene amplification, chromosomal rearrangements may occur, such as the t(11;14) translocation, occurring nearly universally in mantle cell lymphoma (MCL) (19, 20). Overexpression of cyclin D1 also results from the activation of upstream signaling driven by the mitogen-activated protein kinase (MAPK) and NF-kappa-B pathways (21-26). Cyclin D1 regulates cell cycle progression; its overexpression allows transcription of genes

involved in G_1 and S phase progression and permitting DNA replication (27-31). In cells with cyclin D1 overexpression, the transition from the G_1 to S phase is accelerated, leading to increased DNA replication and cell proliferation.

Although cyclin D1 is known to drive cells to enter the S-phase and initiate DNA replication, little is known about how cancer cells adapt to the resultant RS. Cyclin D1 overexpression is nearly ubiquitous in MCL, and approximately 10-20% of other non-Hodgkin lymphomas (NHL) also exhibit this characteristic phenotype (32, 33). Moreover, MCL is known to harbor high chromosomal and genomic instability compared to other NHL (34, 35). While progress has been made in the treatment of MCL, the development of relapsed, refractory disease is common and remains incurable, representing an area of high unmet medical need. We, therefore, utilized MCL as a model system to explore the effects of cyclin D1 overexpression on the induction of RS and DSB repair pathways. We also found that ATM deficiency, the second most common genomic alteration in MCL observed in ~40-50% of cases (36-38), exacerbated CCND1-induced RS, with accumulation of DNA damage in the mitotic-phase of the cell cycle, increasing reliance of MCL cells on MMEJ. Cyclin D1 binds to the *POLQ* gene promoter loci, resulting in increased protein expression of polymerase theta (POLΘ), the primary DNA polymerase of MMEJ(6), to promote the maintenance of genomic integrity in MCL. This increased *POLQ* expression is further increased with concurrent ATM deficiency with cyclin D1 overexpression. Consequently, cyclin D1-expressing MCL cells, particularly those with concomitant ATM deficiency, are vulnerable to POLΘ inhibition, unveiling a potential biomarker-driven treatment option for this patient population.

Results

Cyclin D1 increases DNA replication stress and associated DNA double strand breaks

Before characterizing RS and critical DNA repair pathways in *CCND1*-rearranged MCL cells, we sought to understand the effects of cyclin D1 overexpression in an isogeneic background. *CCND1* cDNA was lentivirally-transduced into U2OS cells, and the cells were assessed for RS markers and DNA damage (Figure 1, A-C). Indeed, cyclin D1-overexpressing U2OS cells exhibited elevated levels of phospho-RPA S33 (p-RPA), a well-established marker for RS,(39) compared with empty vector (EV)-transduced control cells (Figure 1A). This increase in p-RPA correlated with increased DNA DSBs, as evaluated by γ-H2AX (Figure 1B, C). Although higher RS and unrepaired DNA damage are evident in cyclin D1-overexpressing cells, these cells proliferated more rapidly compared with EV-transduced cells (Supplemental Figure 1A). This suggests that cyclin D1-overexpressing cells may depend more heavily on DSB repair pathways to cope with RS, ultimately preventing cell death and facilitating rapid cell growth.

Cyclin D1 overexpression specifically increases MMEJ pathway activity

To study the activation of DSB DNA repair pathways in response to cyclin D1 overexpression, we used U2OS cell-based standardized reporter assays to assess the HR, NHEJ, and MMEJ pathways (40-42). Cyclin D1 was overexpressed in the reporter cells using a lentiviral construct and validated by immunoblotting (Supplemental Figure 1B). These cells exhibited significantly increased MMEJ activity without enhancement of NHEJ or HR, suggesting that cyclin D1-overexpressing cells have specific dependency on MMEJ (Figure 1D).

Given that MMEJ is the major DSB repair pathway activated by cyclin D1 overexpression, we next assessed the localization and accumulation of POLΘ in cyclin D1-overexpressing U2OS

cells. We generated a U2OS clone in which the biallelic N-terminus of the endogenous *POLQ* locus was tagged by a V5 epitope and validated the V5-tagged POLΘ cells through immunoblotting and assessing foci with CRISPR-induced depletion of *POLQ* (Supplemental Figures 1C, 1D and 1E). Indeed, when cyclin D1 was overexpressed in these cells, there was an accumulation of POLΘ foci (Figure 1E) that some co-localized with γ-H2AX foci (Figure 1F). Therefore, the increased DNA damage resulting from cyclin D1 overexpression activated POLΘ recruitment and MMEJ to promote physiologic DSB repair.

MCL cells accumulate unrepaired DNA damage in mitosis, leading to cellular dependence on MMEJ

We next studied RS, DNA damage, and DNA repair in MCL cells carrying the t(11;14) translocation leading to high cyclin D1 expression (43). To delineate the importance of the MMEJ pathway in MCL, we used Jeko cells that carry a 3'-x-FLAG tag at the N-terminus of the endogenous *POLQ* gene and generated isogeneic *POLQ*-deficient cells using CRISPR Cas9 technology (Supplemental Figure 2A). This allowed us to assess the role of MMEJ in MCL by profiling replication-associated physiologic DNA damage in the presence or absence of POLΘ following the synchronization of cells at the G_1/S boundary (Supplemental Figure 2B). Physiologic DNA damage associated with DNA replication begins as the cells enter S phase (Figure 2A). Importantly, this DNA damage was repaired in POLΘ-proficient Jeko cells after they traverse S-phase and enter the mitotic phase of the cell cycle. However, unrepaired DNA damage persisted in mitosis in the absence of POLΘ. This suggests that in MCL cells, MMEJ is critical for resolving replication-associated mitotic DNA damage. In the absence of POLΘ, unrepaired DNA damage accumulates in mitosis, leading to genomic aberrations and cell death (6, 44).

In addition, we assessed RS by probing for p-RPA and for DNA damage through γ-H2AX expression and by the comet assay in *POLQ* control and deficient MCL cells. In the absence of POLΘ, the expression of p-RPA and γ-H2AX significantly increased, with the induction of comet tails. These effects were further enhanced when cells were synchronized in mitosis (Figure 2, B-D). MMEJ, therefore, plays a critical role in MCL in mitigating replication-associated DNA damage, a process that becomes critical in mitosis. Moreover, POLΘ-deficient MCL cells exhibited increased expression of apoptotic markers (e.g., cleaved PARP)(45) along with increased γ-H2AX when synchronized in mitosis (Figure 2E and Supplemental Figure 2C). These data indicate that the inhibition of MMEJ in cyclin D1-overexpressing cells compromises survival, with death likely occurring predominantly in mitosis.

The absence of POLΘ causes chromosomal instability in MCL

Since the accumulation of unrepaired DNA damage in mitosis is more evident with POLΘ deficiency in cyclin D1-high MCL cells, we asked whether reduced POLΘ expression is also associated with chromosomal instability. To address this question, we assessed the number of chromosomal aberrations at a given time in isogeneic wild-type and POLΘ–deficient MCL cells. Indeed, in Jeko cells, the absence of POLΘ caused a significant increase in chromosomal aberrations (double minute chromosomes and dicentric chromosomes) correlating with the increased levels of RS, unrepaired DNA damage during mitosis, and with increased expression of apoptotic markers (Figure 2, E-G).

The absence of POLΘ in MCL causes RS by increasing single-strand DNA gaps and confers sensitivity to ATR or PARP inhibition

Given the increased RS in MCL cells lacking POLΘ, we assessed the effects of POLΘ deficiency on DNA replication using DNA fiber assays. POLΘ–deficient MCL cells

demonstrated a significant increase in single-strand DNA gaps, compared to POLΘ-proficient isogeneic cells (Figure 2, H-I). Since single-strand DNA gaps exacerbate RS and are detrimental to cell proliferation and survival and suggests a mechanism for RS-induced apoptosis in POLΘ-deficient MCL cells (2, 46).

We also looked at the susceptibility of POLΘ-deficient cells to ATR inhibition, a key kinase known to promote the resolution of RS (2). Confirming the heightened RS in POLΘ-deficient MCL cells, these cells showed increased sensitivity to ATR inhibition compared to POLΘ-proficient MCL cells (Supplemental Figure 2D). We also asked whether POLΘ-deficiency conferred PARP inhibitor sensitivity. Parental Jeko cells are HR repair-proficient and PARP inhibitor resistant (47). However, PARP inhibitors can increase RS by trapping PARP on DNA(48), accelerating replication fork speed,(49) and impeding the maturation of nascent DNA strands (50). Indeed, the PARP inhibitor, Olaparib reduced the viability of POLΘ-deficient cells, whereas control cells were unaffected (Supplemental Figure 2E). These results further confirm the increased RS experienced by HR-proficient MCL cells in the absence of POLΘ that exceeds a lethal threshold upon challenge with ATR or PARP inhibition.

Cyclin D1 promotes MMEJ by directly upregulating *POLQ* promoter activity

Since *CCND1* is an essential gene for MCL, its CRISPR knockout is lethal at the cellular level. Therefore, we used CRISPR interference (CRISPRi) technology to stably decrease the expression of cyclin D1 (51). As depicted in Figure 3A, we generated a stable knockdown of cyclin D1 in Jeko cells, in which the endogenous *POLQ* gene is tagged with 3xFLAG. The decreased expression of cyclin D1 had a minimal effect on cell cycle progression (Supplemental Figure 3A). Interestingly, we observed that decreased cyclin D1 expression also resulted in decreased POLΘ protein and *POLQ* mRNA expression and decreased physiologic DNA

damage (Figure 3A and B). Similarly, engineered MCL cells carrying the MMEJ reporter confirmed that decreased expression of cyclin D1 reduced MMEJ-mediated DSB repair (Figure 3C). Cells with reduced cyclin D1 expression were also less sensitive to pharmacologic POLΘ inhibition (Figure 3D).

To confirm the results obtained in the MCL cells, cyclin D1 was ectopically overexpressed in other NHL cell lines, followed by measurement of *POLQ* expression via qPCR. As predicted, a significant increase in *POLQ* transcripts was observed in other NHL cell lines overexpressing cyclin D1 (Figure 3E), suggesting that our results may apply to other malignancies harboring cyclin D1 overexpression.

Following observing increased *POLQ* gene expression when cyclin D1 is overexpressed, we investigated whether cyclin D1 directly binds to the *POLQ* promoter (52). To explore this possibility, we overexpressed HA-tagged cyclin D1 in Jeko cells with knocked-down endogenous cyclin D1 (Supplemental Figure 3B) and U2OS cells (Supplemental Figure 3C) and performed chromatin immunoprecipitation with an anti-HA antibody, followed by qPCR. The ATM gene was utilized as a negative control because alterations in cyclin D1 expression did not affect ATM gene expression in either U2OS or Jeko cells (Supplemental Figures 3D and 3E). We found that cyclin D1 directly binds to the *POLQ* promoter (Figure 3F, Supplemental Figure 3, F and G). Subsequently, we determined the transcriptional activity of the *POLQ* promoter using a luciferase assay. After normalizing the transfection efficiency with Renilla activity, *POLQ* promoter-driven Firefly luciferase activity was significantly increased in HEK cells when cyclin D1 was overexpressed (Figure 3G). These data indicate that cyclin D1 binds to the *POLQ* promoter and enhances its transcriptional activity, leading to upregulation of *POLQ* gene expression.

Enhancement of replication stress by concomitant depletion of ATM

Approximately 45% of MCLs harbor ATM deficiency (36-38, 53). ATM regulates the DNA damage response, and its absence may reroute more DSB repair to the MMEJ pathway (54). Given this clinical and therapeutic relevance, we determined whether ATM deficiency could further increase RS and DSB repair pathway dependency, specifically in cyclin D1-overexpressing cells. Indeed, ATM deficiency in cyclin D1-overexpressing U2OS cells exacerbated RS, as assessed by increased p-RPA (Figure 4A). As expected, the increased RS was associated with increased γ-H2AX expression (Figure 4B).

We next validated this finding in MCL by using our isogeneic Jeko cells treated with an ATM inhibitor. When POLΘ deficient Jeko cells were treated with the ATM inhibitor AZD0156 (55), a significant increase in unrepaired mitotic DNA damage was observed, compared to vehicle-treated wild-type and POLΘ deficient cells (Figure 4C). Furthermore, a significant increase in p-CHK1, a validated biomarker for replication stress(2), was detected when POLΘ deficient Jeko cells were treated with AZD0156; this increased p-CHK1 was more evident when cells were synchronized in mitosis (Figure 4D).

Using the U2OS cells engineered with DNA repair pathway reporters, we assessed HR, NHEJ, and MMEJ activity in cyclin D1-overexpressing cells in both ATM-proficient and ATM-deficient backgrounds (Supplemental Figure 4A-C). The upregulation of the MMEJ pathway that occurred with cyclin D1 overexpression was further enhanced by concomitant ATM deficiency, suggesting an increased dependency of these cells on MMEJ when ATM is absent (Figure 4E). The activity of the HR and NHEJ repair pathways was not increased with cyclin D1 overexpression and ATM deficiency, suggesting that these co-occurring alterations uniquely upregulate MMEJ, dictating MMEJ dependence for DSB repair. (Supplemental Figure 4, I and J).

We then assessed the *POLQ* expression in MCL in relation to ATM alteration using isogeneic Mino cells. In ATM deficient Mino cells, *POLQ* expression significantly increased when compared to ATM proficient cells (Figure 4F, Supplemental Figure 4D). This observation was further confirmed in cyclin D1 overexpressed U2OS cells with and without ATM deficiency (Supplemental Figure 4, A and E). After confirming in isogeneic cell lines, we then studied *POLQ* expression in primary MCL cells. The *POLQ* expression was increased in primary ATM deficient primary MCL cells which was further confirmed by publicly available MCL gene expression dataset which showed significant increased *POLQ* expression with no change to CCND1 expression levels in ATM mutated MCL compared to ATM wild-type MCL (Supplemental Figure 4, F-H) (56). Taken altogether, this data indicates that in cells with cyclin D1 overexpression, especially in MCL, ATM deficiency further leads to increased expression of *POLQ* compared to ATM-proficient cells.

Consistent with increased *POLQ* gene expression when ATM is deficient in the background of cyclin D1 overexpression, POLΘ protein expression in cyclin D1-overexpressing cells was further enhanced by ATM deficiency (Figure 5A). Furthermore, the accumulation of POLΘ as foci into replication-induced DNA damage sites was significantly increased with concomitant cyclin D1 overexpression and ATM deficiency compared to cells with monogenic altered counterparts (Figure 5, B and C). These data suggest that ATM deficiency exacerbates RS in cyclin D1-overexpressing cells, with consequent DNA damage causing increased MMEJ dependence.

Genetic and pharmacologic MMEJ pathway disruption has antiproliferative effects in MCL cells

Next, we explored targeting POLΘ as a therapeutic strategy in MCL. To assess the impact of POLΘ on cell proliferation and survival, we conducted a competitive proliferation assay in different MCL cell lines after knocking out *POLQ*. *POLQ* genetic depletion caused dampening of cell proliferation in all cell lines tested, with the Granta and UPN2 cell lines being more sensitive compared to the Jeko, JVM-2, and Z138 cell lines (Figure 6A and Supplemental Figure 5A). Subsequently, we used two independent POLΘ inhibitors, novobiocin (NVB), an inhibitor of the helicase domain (57), and ART558, an inhibitor of the polymerase domain(58), to validate this antitumor effect in multiple MCL cell lines (Figure 6, B and C). All MCL cell lines were sensitive to both POLΘ inhibitors; again, Granta and UPN2, as well as MCIR cells which are ATM deficient MCL cell lines, demonstrating relatively more sensitivity. Consistent with our observations of increased RS and MMEJ pathway dependence when ATM is depleted in cyclin D1-overexpressing cells, ATM-deficient cell lines were hypersensitive to POLΘ inhibition (Supplemental Figure 5B).

To assess the effect of ATM inhibition in a POLΘ-deficient background in MCL, we performed the competitive assay using isogeneic cells with *ATM* and *POLQ* deficiency. Indeed, as shown in Figure 6D, *POLQ* depletion, but not *ATM* depletion, significantly decreased the proliferation of Jeko cells. The simultaneous depletion of *ATM* with *POLQ* significantly increased the anti-proliferative and pro-apoptotic effects, compared to *POLQ* depletion alone. We also generated isogeneic ATM depleted MCL cells in the Mino cell line, an *ATM* wild-type cell line. ATM-deficient Mino cells were more sensitive to pharmacologic inhibition of POLΘ with NVB than ATM-proficient Mino cells (Figure 6E). Furthermore, co-treatment of ATM-proficient Jeko cells with an ATM inhibitor AZD0156 (ATM inhibitor) and ART558 (POLΘ inhibitor) caused synergistic antitumor activity (Figure 6F and G, average synergy Bliss score 72.91**)**. Conversely, isogeneic

POLQ-depleted Jeko cells were more sensitive to AZD0156-mediated ATM inhibition than *POLQ*-proficient Jeko cells (Figure 6H).

In addition to validating the enhanced antitumor effect with *POLQ* depletion in cyclin D1-overexpressing and ATM-deficient MCL, we also recapitulated this effect using U2OS cells. Indeed, cyclin D1-overexpressing cells were more sensitive to POLΘ inhibition by ART558 and NVB. Additionally, pharmacologic POLΘ inhibition had a greater antitumor effect in cyclin D1-overexpressing cells lacking ATM, compared with CCND1-overexpressing cells that were ATM-proficient (Supplemental Figure 5, C and D). Taken together, our data indicate that ATM-deficient MCL cells are especially sensitive to POLΘ inhibition. These results may broadly apply to other cyclin D1-overexpressing tumor cells that are also ATM-deficient, as a similar phenotype was also seen in U2OS cells, an osteosarcoma cell line. In contrast, cyclin D1-overexpressing tumor cells that are ATM-proficient may be highly vulnerable to combined POLΘ and ATM inhibition.

POLΘ inhibition produces significant antitumor effects in MCL *in vivo*

To examine the in vivo efficacy of POLΘ inhibition in MCL, immunodeficient mice were subcutaneously engrafted with isogeneic ATM-deficient ($ATM^{-/-}$) and ATM-proficient ($ATM^{+/+}$) Mino cells. Intraperitoneal NVB treatment commenced twice daily after tumor engraftment ($100mm^3$). Tumor growth was significantly reduced in ATM-proficient Mino xenografts treated with NVB compared to vehicle (Figure 7A). However, tumor growth inhibition was enhanced considerably in ATM-deficient Mino xenografts. No treatment-related morbidity or mortality was seen in the mice, and animal weights were similar in all groups (Supplemental Figure 6). Moreover, overall survival significantly increased in mice bearing ATM-proficient Mino

xenografts treated with NVB (Figure 7B), which was further enhanced in ATM-deficient xenografts. Histopathological analyses showed a significant increase in RS marked by p-RPA32 S4/S8 (Figure 7, C and D) and unrepaired DNA damage evidenced by γ-H2AX (Figure 7, E and F) in ATM-proficient xenografts treated with NVB, and these biomarkers were further increased in NVB-treated ATM-deficient xenografts.

POLΘ inhibition reduces the viability of primary MCL cells

Having validated the effect of POLΘ inhibition in MCL using human cell lines, we next assessed the dependence on *POLQ* expression of primary tumor cells from patients with NHL. MCL exhibited the highest expression of cyclin D1 compared to most other NHL subtypes (Figure 8A, Supplemental Figure 7A). Consistent with our finding that cyclin D1 overexpression increases *POLQ* expression in cells, MCL primary cells exhibited the highest *POLQ* expression compared to other types of NHL, such as follicular lymphoma (FL), chronic lymphocytic leukemia/small lymphocytic lymphoma (CLL/SLL), marginal zone lymphoma (MZL), and diffuse large B-cell lymphoma (DLBCL), where cyclin D1 overexpression is not commonly observed (Figure 8B).

Subsequently, we tested the antitumor activity of POLΘ inhibition in primary MCL cells. Treatment of primary cells obtained from 24 MCL patients with ART558 showed significantly compromised viability (Figure 8C). Indeed, validating our cell line data, primary MCL cells with ATM deficiency were more affected by ART558 compared to ATM proficient primary MCL cells (Figure 8D, Supplemental Figure 7B). As in the MCL cell lines, simultaneous inhibition of ATM and POLΘ showed enhanced antitumor activity in primary ATM-proficient MCL primary cells compared to POLΘ inhibition alone (Figures 8, E and F). In summary, these results in primary MCL cells confirm that inhibition of POLΘ is effective for *ATM*-mutated MCL, and that

concurrent inhibition of ATM and POLΘ is a promising therapeutic strategy for ATM-proficient MCL.

Discussion

Our study demonstrates that overexpression of cyclin D1 increases RS, amplifying the reliance of cells on the MMEJ pathway for repairing DNA replication-associated DNA damage, particularly during the mitotic phase of the cell cycle. This reliance intensifies with ATM deficiency. Moreover, cyclin D1 directly upregulates *POLQ* expression, which is further augmented by ATM deficiency. This heightened dependence on MMEJ may hold significance in cancers with high cyclin D1 expression, notably MCL, presenting a promising target for therapeutic intervention.

CCND1 is one of the most amplified genes in human cancers but its effects on RS and DNA damage repair have not been extensively characterized. Our study demonstrates that cyclin D1 overexpression induces RS in the context of MCL. Although *CCND1* is an oncogene known for its cell cycle regulatory function,(18) recent studies have also identified the direct binding ability of cyclin D1 to gene enhancers, affecting respective gene transcription (52, 59). Here, we have demonstrated that cyclin D1 directly binds to the *POLQ* promoter and enhances *POLQ* transcription, indicating that MMEJ is likely required for the genomic integrity and survival of cyclin D1-overexpressing cells. The impact of these findings may extend beyond MCL, as cyclin D1 overexpression is seen in about 10-20% of NHL and other hematologic malignancies(33), as well as in solid tumors, including 50% of breast and colon cancers,(60, 61) and in ~80% of pancreatic cancer (62). Therefore, assessment of RS and MMEJ pathway dependence may be warranted in these other tumor types driven by oncogene expression.

Additionally, our results illustrate the synergistic interaction between POLΘ and ATM deficiencies in cells overexpressing cyclin D1, which is significantly stronger compared to cells with lower levels of cyclin D1 expression. Although previous studies in mice have indicated that concurrent deficiencies in POLΘ and ATM can be partially synthetic lethal (63), our data suggest that cyclin D1 overexpression may be a useful biomarker for combined POLΘ and ATM inhibition in cancer treatment. Furthermore, unlike in MCL, inhibiting POLΘ in ATM-deficient models that are BRCA-proficient without elevated cyclin D1 expression demonstrated only a minimal additive effect (64). Our data support these findings, showing that ATM depletion in cells that do not overexpress cyclin D1 had minimal impact on RS and MMEJ dependence.

Notably, a synergistic antitumor effect from the simultaneous inhibition of ATM and POLΘ was observed only in settings with cyclin D1 overexpression in an HR repair proficient background. This mechanistic insight highlights a distinct disruption of DNA replication and variations in DSB repair pathway dependency in ATM-deficient, HR-proficient cells with cyclin D1 overexpression. Consequently, our findings may have broader implications for other HR-proficient cancers exhibiting concurrent cyclin D1 overexpression and ATM deficiency, and suggest a biomarker-driven approach for the development of inhibitors of POLΘ.

Previous studies have demonstrated that POLΘ is essential for sealing post-replicative single-strand DNA gaps in BRCA-deficient cancer cells (64, 65). Additionally, the function of POLΘ has been linked to maintaining genomic stability in HR-deficient solid tumor malignancies (64). To our knowledge, no studies have examined the role of POLΘ in maintaining chromosomal stability in hematologic malignancies characterized by cyclin D1 overexpression, particularly in HR-proficient backgrounds. Our results indicate that POLΘ is crucial for reducing DNA replication stress, especially in HR-proficient cells subjected to perturbations in oncogenes and

tumor suppressor genes, including *CCND1* and *ATM*. Moreover, highly proliferative MCL are highly dependent on MMEJ-mediated DSB repair during the mitotic phase of the cell cycle, consistent with previous studies that demonstrated the activation of POLΘ by PLK1 and the role of MMEJ in repair of damaged DNA during mitosis (5, 6). However, considering POLΘ's role in sealing single-strand DNA gaps predominantly during the S-phase of the cell cycle (64, 65), it is important to note that POLΘ's functions are not restricted to mitosis. It also should be active in the S-phase, even in cells with high HR proficiency. These findings are significant to the field of malignant hematology, where, despite the high proliferative index of cancer cells, the biology of RS and mechanisms of DNA damage repair remain understudied (66).

Our study has limitations, particularly related to the exact mechanism for the increased MMEJ dependence resulting from ATM depletion in cyclin D1-overexpressing cells. Although we found that ATM deficiency further increase *POLQ* transcription in cyclin D1 overexpressed cells, the exact mechanism behind this observation needs to be elucidated. Previous studies have shown that ATM suppresses MMEJ by regulating DNA-end degradation and controlling the activity of the Mre11 nuclease, which is essential for initiating MMEJ (54). Consequently, ATM deficiency leads to increased DNA end resection, promoting the use of MMEJ for double-strand break repair (54).

It is unlikely that the increased POLΘ protein expression we observed with cyclin D1 overexpression—an effect further heightened by ATM deficiency—is merely a consequence of cell cycle effects related to cyclin D1 overexpression or ATM deficiency. In our experimental system, neither cyclin D1 overexpression nor ATM deficiency significantly altered the cell cycle dynamics of the malignant cells. Although its function is most critical during mitosis, POLΘ protein levels are relatively lower in the mitotic phase compared to other cell cycle stages (5, 6).

Importantly, ATM deficiency does not induce cell cycle arrest, while cyclin D1 overexpression is expected to enhance cell cycle progression from the G_1 to the S phase. Consequently, our findings of increased *POLQ* expression in the context of cyclin D1 overexpression and ATM deficiency appear to be a direct result of these genetic alterations rather than a secondary effect stemming from cell cycle perturbations.

In conclusion, our work elucidates the impact of cyclin D1 overexpression on RS, particularly emphasizing its implications for MCL. We identified POLΘ as a critical mediator in the cellular management of RS induced by cyclin D1 overexpression, consequently decreasing the prevalence of single-stranded DNA and increasing cellular dependency on MMEJ-mediated DSB repair, particularly during the mitotic phase. This process is essential for maintaining cell proliferation and viability. Moreover, the concurrent reduction of ATM in the context of cyclin D1 overexpression, even in an HR-proficient background, exacerbates RS, leading to enhanced POLΘ expression and even greater reliance on MMEJ. These preclinical results demonstrate the therapeutic potential of targeting POLΘ in oncogene-driven hematologic cancers, especially in MCL, where cyclin D1 overexpression is ubiquitous and ATM deficiency is common, but may extend to other oncogene-driven hematologic cancers. Further, these preclinical data strongly support bringing our findings from the bench to the bedside for relapsed and/or refractory MCL targeting the MMEJ pathway through POLΘ inhibition with or without ATM inhibition.

Methods

Sex as a biological variable

We included both male and female animals in our study and the findings were consistent across both sexes.

Cell Culture

U2OS (ATCC, HTB-96), HEK293T (ATCC, CRL-3216), UPN2(67) , and Granta-519 (DSMZ, ACC 342) cells were cultured in Dulbecco's Modified Eagle's Medium (DMEM, Gibco). RPE cells (ATCC, CRL-4000) were cultured in DMEM/F-12 (Gibco). Jeko (ATCC, CRL-3006), Mino (ATCC, CRL-3000), JVM-2 (ATCC, CRL-3002), Rec1 (ATCC, CRL-3004), and MCIR cells (68) were cultured in Roswell Park Memorial Institute-1640 (RPMI-1640) medium (Gibco). Z138 cells (ATCC, CRL-3001) were cultured in Iscove's Modified Dulbecco's Medium (IMDM, Gibco). All media were supplemented with 10% fetal bovine serum (FBS, Sigma-Aldrich) and 1% penicillin/streptomycin (Life Technologies). Cells were maintained at 37°C in a humidified incubator with 5% CO_2.

Lentivirus-mediated gene manipulation

For overexpressing CCND1 in cells, 2xHA-tagged CCND1 was integrated into a pLV-EF1a-IRES-Blast vector (addgene #85133), and cells were lentivirally transduced with control or CCND1. After blastidicin selection for 96hr, cells were used to perform experiments.

For CRISPR-mediated gene knockout, cells were lentivirally transduced with Cas9 and a sgRNA simultaneously by using a lentiCRISPR v2 vector (addgene #52961). After puromycin selection for 72hr, cells were used to perform experiments.

For CRISPR interference (CRISPRi)-mediated gene knockdowns, cells were transduced with dCas9-KRAB using the lentivirus generated by pHR-SFFV-KRAB-dCas9-P2A-mCherry

(addgene #60954). mCherry-positive cells were sorted by FACS Aria II (BD biosciences), and subsequently transduced with a control (NT) or sgRNA targeting CCND1 using the lentivirus generated by lentiguide-puro vector (addgene #52963). After puromycin selection for 72hr, cells were used to perform experiments.

For competitive assay, Cas9-expressing cells were lentivirally transduced with a control or sgRNA targeting *POLQ* in a pLKO5.sgRNA.EFS.GFP vector (addgene #57822) with or without a control or sgRNA targeting *ATM* in a pLKO5.sgRNA.EFS.tRFP657 vector (addgene #57824).

Lentivirus was produced by transient transfection of HEK293T cells with viral plasmids along with gag-, pol- (psPAX2, addgene #12260), and env- (pMD2.G, addgene #12259) expressing plasmids using the calcium-phosphate method (Takara Bio).

Sequences of the sgRNA used for CRISPR-mediated gene knockout or gene silencing in this study are provided in Supplemental table 1.

Generation of CRISPR-mediated knockout and knock-in cells

For generating *ATM* or *POLQ* knockout cells, a ribonucleoprotein (RNP) complex was formed by Alt-R™ S.p. HiFi Cas9 and CRISPR-Cas9 sgRNA targeting *ATM* or *POLQ* (Integrated DNA Technologies). MCL cells were resuspended in SF Nucleofector Solution with supplement (Lonza) and then mixed with the Cas9/sgRNA RNP complex and Alt-R™ Cas9 Electroporation Enhancer (Integrated DNA Technologies), respectively. The Cas9/sgRNA RNP complex was delivered to the cells by 4D-NucleofectorTM (Lonza).

For generating endogenously 3xFLAG-tagged *POLQ* Jeko or V5-tagged *POLQ* U2OS knock-in cells, the Cas9/sgRNA RNP complex together with a template was delivered. Jeko and U2OS cells were resuspended in SF or SE Nucleofector Solution with supplement (Lonza), respectively. The double-stranded DNA template consists of 500bp upstream and 500bp downstream of the cutting site by Cas9 together with a 3xFLAG tag or V5 tag. Of note, the

codon usage of *POLQ* residue 6R of the template DNA was changed from CGG to CGT to destroy the PAM sequence, which prevents the inserted template from being cut by Cas9 after knock-in. After electroporation, the cells were incubated for 24 hours with an HDR enhancer (Integrated DNA Technologies) to increase knock-in efficiency. Media was changed the following day, and then 2 days after cells were seeded in a 96-well plate to isolate single clones. Individual clones were tested for genomic editing analyses using immunoblotting and genomic PCR with subsequent Sanger sequencing. The sgRNA used for gene knockout and knock-in are mentioned in the **Supplemental Table 1**

Viral transduction

Retroviruses for mouse cells were produced by transient transfection of Plat-E packaging cells with retroviral constructs using the calcium-phosphate method12. Retroviruses for human cells and lentiviruses were produced by transient transfection of 293T cells with viral plasmids along with gag-, pol-, and env-expressing plasmids using the calcium-phosphate method10. Retrovirus transduction to the cells was performed using Retronectin (Takara Bio Inc, Otsu, Shiga, Japan).

Western Blot Analysis

Primary antibodies used were anti-CCND1 (rabbit polyclonal; CST, catalog #2922S), anti-ATM (rabbit monoclonal; CST, catalog #2873S, clone D2E2), anti-g-H2AX (rabbit monoclonal; CST, catalog #9718S, clone 20E3), anti-RPA (rabbit polyclonal; CST, catalog #52448), anti-p-RPA-S8 (rabbit monoclonal; CST, catalog #54762, clone D6X3V), anti-cleaved-PARP (rabbit monoclonal; CST, catalog #5625T, clone D64E10), anti-cyclin-B1 (rabbit polyclonal; CST, catalog #4138S), anti-CHK1 (mouse monoclonal; CST, catalog #2360S, clone 2G1D5), anti-pCHK1(rabbit monoclonal; CST, catalog #2348, clone 133D3), anti-KAP1 (mouse monoclonal; Abcam, catalog #ab22553, clone 20C1), anti-pKAP1 (rabbit polyclonal; Abcam, catalog

#ab70369), anti-V5 (rabbit monoclonal; CST, catalog #13202, clone D3H8Q), anti-Flag (mouse monoclonal; Sigma Aldric, catalog #F1804, clone M2), anti-a-tubulin (rabbit monoclonal; CST, catalog #2125, clone 11H10), anti-B-actin (rabbit monoclonal; CST, catalog #4970, clone 13E5), anti-vinculin (rabbit monoclonal; CST, catalog #13901, clone E1E9V), and anti-GAPDH (rabbit monoclonal; CST, catalog #5174, clone D16H11).

Reverse transcription PCR (RT-PCR)

Total RNA was extracted using RNeasy Mini Kit (QIAGEN). Complementary DNA synthesis was performed using SuperScript IV First-Strand cDNA Synthesis Reaction (Thermo Fisher Scientific). Quantitative PCR (qPCR) was performed using Power SYBR Green PCR Master Mix (Thermo Fisher Scientific) and Quant Studio 7 flex Real-Time PCR System (Thermo Fisher Scientific). ΔCt was calculated using *GAPDH* as a control and normalized to control cell lines if not otherwise specified in a figure legend. RT-qPCR assays were performed in technical triplicate. Sequences of the primers used for RT-qPCR:

hCCND1-qF1: TCTACACCGACAACTCCATCCG
hCCND1-qR1: TCTGGCATTTTGGAGAGGAAGTG
hPolQ-qF1: CTTGTGGCATCTCCTTGGAGCA
hPolQ-qR1: AATCCCTTGGCTGGTCTCCATC
hATM-qF1: TGTTCCAGGACACGAAGGGAGA
hATM-qR1: CAGGGTTCTCAGCACTATGGGA

DNA repair template assay

U2OS cells carrying a DNA repair template reporter (DR-GFP, EJ5-GFP, and MMEJ-GFP) were lentivirally transduced with Cas9 and sgRNA (co-expressing puromycin resistance gene) with or without a control vector or CCND1 cDNA (co-expressing blasticidin resistance gene). After puromycin and blasticidin selection, 40,000 DNA repair template reporter cells were seeded in 12-well plates and adenovirally transduced with Isce-I the following day. 48h after Isce-I transduction, GFP signals were analyzed by CytoFLEX (Beckman). The signals were normalized to control cells. DR-GFP and EJ5-GFP cells were kind gifts from Dr. Jeremy Stark

(CITE PAPERS). MMEJ-GFP cells were generated by lentivirally transducing a cassette into U2OS cells using a pLV-EF1a-IRES-puro vector (addgene #85132) as previously described (ref. PMID: 23610439).

Competitive assay

Mantle cell lymphoma cell lines were lentivirally transduced with Cas9 (co-expressing mCherry), and mCharry positive cells were by FACS Aria II (BD biosciences). These mCherry positive cells were subsequently lentivirally-transduced a sgRNA targeting control or *POLQ* (co-expressing GFP) together with a sgRNA targeting control or *ATM* (co-expressing tRFP657) and were monitored changes in the frequency of GFP/tRFP657 double positive cells. GFP and tRFP657 signals were analyzed by CytoFLEX (Beckman) every 3-4 days. The signals were normalized to the frequency of GFP-positive or GFP/tRFP657 double positive cells at day3.

Cell survival assays

For the clonogenic assay, 500 to 4,000 cells were seeded into 6-well plates, with the exact number adjusted based on the growth rate of each cell line. The following day, cells were treated as indicated. After 7–14 days, colonies were washed with PBS, fixed with methanol:acetic acid (3:1) fixation solution for 1 hour, and stained with 0.5% crystal violet (prepared in 10% methanol) for 1 hour. Stained plates were then imaged and analyzed using ImageJ (Version 1.54, National Institutes of Health, Bethesda, MD, USA).

For the CellTiter-Glo assay, cells were plated in 96-well plates and treated as indicated the following day. After 5–7 days, CellTiter-Glo reagent (Promega, catalog #G7573) was added according to the manufacturer’s protocol to assess cell viability. Luminescence was measured using a plate reader.

Chromosomal breakage assay

Jeko control or sg*POLQ* cells were exposed to 5 ng/mL MMC for 48 h. Cells were treated with 100 ng/mL of colcemid for 2 h, followed by a hypotonic solution (0.075 M KCl) for 20 minutes and fixed with 3:1 methanol/acetic acid. Slides were stained with Wright's stain and 50 metaphase spreads were scored for aberrations.

Immunofluorescence

After specific treatments or in the absence of treatment, cells were fixed with 4% paraformaldehyde for 15 minutes at room temperature. Cells were then permeabilized with 0.3% Triton X-100 for 10 minutes on ice, followed by blocking with 3% non-fat milk for 1 hour at room temperature. The slides were stained with primary antibodies at 4℃ overnight. Afterward, they were stained with secondary fluorescent-conjugated antibodies for 1 hour at room temperature. The slides were scanned using fluorescence microscope. At least 100 cells were counted for each sample. Foci quantification was performed using software CellProfiler version 4.2.6.

Primary antibodies used were anti-g-H2AX (mouse monoclonal; MilliporeSigma, catalog # 05-636-MI, clone JBW301), anti-p-RPA2-S33 (rabbit polyclonal; Novus Biologicals, catalog # NB100544), and anti-V5 (rabbit monoclonal; CST, catalog #13202, clone D3H8Q).

Comet Assay

The alkaline comet assays were performed to detect both single and double-stranded DNA breaks. 1000 cells, suspended in PBS, were mixed with 50µl melted low melting agarose and pipetted onto the Cometslides (R&D Systems, Catalog: #4250-050-K). Once the agarose solidified, the slides were immersed in a lysis solution for 18 hours to facilitate cell lysis. Following lysis, the slides were incubated in an alkaline unwinding solution for 1 hour to denature the DNA. Electrophoresis was performed at 21 V for 45 minutes in an alkaline

electrophoresis solution. The slides were stained with SYBR green solution, scanned by fluorescence microscope, and analyzed using CometScore software (Version 2.0).

DNA fiber assays with S1 nuclease

For DNA fiber assays, cells (sgNT and sg*POLQ* Jeko cells) s were seeded at 50% confluence in six-well plates one day before the experiment. The next day, they were sequentially incubated with CldU (100 µmol/L, 30 minutes) followed by IdU (100 µmol/L, 2 hours) at 37°C. After each incubation step, cells were washed three times with PBS and permeabilized using CSK buffer (0.5% Triton X-100, 10 mmol/L HEPES, 300 mmol/L sucrose, 100 mmol/L NaCl, and 3 mmol/L $MgCl_2$) for 10 minutes at room temperature. Following a wash with S1 nuclease buffer (50 mmol/L NaCl, 300 mmol/L sodium acetate pH 4.6, 10 mmol/L zinc acetate, and 5% glycerol), cells were incubated at 37°C for 30 minutes in the presence or absence of S1 nuclease (20 U/mL). Nuclei were then washed with PBS, resuspended in PBS with 0.1% BSA, harvested using a cell lifter, pelleted, and mixed with melted agarose to form plugs by incubating at 4°C for 45 minutes. These plugs were then digested overnight at 50°C in proteinase K solution before being washed four times with buffer and incubated in combing buffer overnight at 4°C. DNA fibers were stretched onto coverslips (#COV002-RUO) using the FiberComb Molecular Combing System (#MCS001) and processed for immunostaining. Coverslips were incubated overnight at 37°C with rat anti-BrdU (Abcam, #ab6326, clone BU1/75 (ICR1)) and mouse anti-BrdU (BD Biosciences, #347580, clone B44), both diluted in BlockAid (Invitrogen, #B10710), followed by goat anti-rat Cy5 (Abcam, #ab6565, polyclonal) and goat anti-mouse Cy3 (Abcam, #97035, polyclonal) for 45 minutes at 37°C. To detect single-stranded DNA, samples were further incubated with mouse anti-ssDNA antibody (DSHB autoanti-ssdna) for 1 hour and 15 minutes at 37°C, followed by goat anti-mouse BV480 (Jackson, #115-685-166, polyclonal) for 45 minutes at 37°C. After immunostaining, coverslips were air-dried, mounted, and scanned using the FiberVision scanner (Genomic Vision).

Cell Cycle Synchronization and Cell Cycle Analysis

Cells were synchronized at the G1/S boundary using a double thymidine block. cells were first treated with 2 mM thymidine for 16 hours, followed by release into fresh thymidine-free medium for 8–10 hours to allow progression through the cell cycle. Cells were then subjected to a second 2 mM thymidine treatment for another 16 hours, ensuring a more uniform synchronization at the G1/S transition. Mitotic synchronization was achieved using nocodazole (100 ng/mL, 12 hours) or RO3306 (8μM, 18 hours) followed by a 1-hour release in fresh medium. Cells were fixed in 70% ethanol, stained with propidium iodide, and analyzed by flow cytometry to determine cell cycle distribution.

Luciferase assay

HEK293T cells were seeded in 12-well culture plates at a density of a hundred thousand per well. At 16h after seeding, the cells were transfected with pGL4.1 *POLQ* promoter (co-expressing Firefly Luciferase [FLuc]), pLV-IRES-Blast empty vector or pLV-IRES-Blast CCND1, and pGL4.71 vector (co-expressing Renilla Luciferase [RLuc]) using Lipefectamine LTX Reagent with PLUS Reagent (Thermo Fisher Scientific). The cells were harvested 48 h after transfection and were assayed for the luciferase activity by means of the luciferase assay system (Promega) and a luminometer (BMG LABTECH, FLUOstar OPTIMA). Promoter activity was calculated by ratio of Rluc to Lluc.

ChIP-qPCR assay

CRISPRi-mediated CCND1 knocked down Jeko cells were lentivirally transduced with an empty vector or 2xHA-Thirty-million Jeko control or CCND1 knockdown cells were ChIP was performed using Simple chip kit (Cell signaling technology, #9002) with an antibody against HA (abcam, catalog #ab9110, polyclonal) following the manufacturer’s recommendations. Purified

DNA was then subjected to quantitative RT-PCR using a SYBR Select Master Mix (Applied Biosystems). Sequences of the primers used for ChIP-qPCR:

POLQ #1-F GAGCTACTTCCCTGATCTACCT
POLQ #1-R CCATACTGACCTAAAAGCCTTCC
POLQ #2-F AGCATGGCCTTCCTATTCAAAC
POLQ #2-R CTAAGACTTCCGGCCTCCAA
POLQ #3-F TTGGAGGCCGGAAGTCTTAG
POLQ #3-R ATCTTCCCGCCAGTCTTCAA
POLQ #4-F CGAGTCTATGGCTTTCGGGT
POLQ #4-R TTCCCGCCAGTCTTCAAACT
ATM #1F AATCGCTTCCGCCTAGAGAAAG
ATM #1R CTCTCACCCACCCTCTTCGC
ATM #2F GTCGTCACCTTCGTCCGCAG
ATM #2R GCCTGCGCCATGTCCAC

Animal experiment

All animal experiments were conducted in accordance with Institutional Animal Care and Use Committee-approved protocols at Dana-Farber Cancer Institute. One million *ATM*-wildtype or *ATM*-knockout Mino cells were subcutaneously injected into 7-week-old male and female NOD.Cg-*Prkdc*^{scid} Il2rg^{tm1Wjl}/SzJ mice, purchased from the Jackson laboratory. Male and female mice were used in a 1:1 ratio, and each treatment group had eight mice (four males and four females). After confirming tumor engraftment, mice were treated with NVB (75 mg/kg) or PBS twice a day via intraperitoneal injection (IP injection) for 3-4 week. Tumors were measured every 2 to 3 days using an electronic caliper, and tumor volumes were calculated by using the formula L×W×W/2. For immunohistochemistry analysis, tumors were excised and fixed with formaldehyde. Mice with a tumor of more than 20 mm in length or width were euthanized.

Primary patient samples analysis

Primary patient samples were obtained from the Mayo Clinic Lymphoma Predolin Biobank. Primary cells (20,000 per well) were plated in 96 well plates in triplicates and conducted CellTiter-Glo assay. On selected patients where sufficient cells were obtained, immunoblotting was conducted to assess for ATM deficiency (rabbit monoclonal; CST, catalog #2873S).

Immunohistochemistry

Immunohistochemistry was performed on the Leica Bond III automated staining platform using the Leica Biosystems Refine Detection Kit (Leica; DS9800). Formalin-fixed paraffin-embedded (FFPE) tissue sections were baked for 30 minutes at 60°C and deparaffinized (Leica AR9222) prior to staining. Primary antibodies were incubated for 30 minutes, visualized via DAB, and counterstained with hematoxylin (Leica DS9800). The slides were rehydrated in graded alcohol and cover slipped using the HistoreCore Spectra CV mounting medium (Leica 3801733).

Antibodies: 1) Phospho-RPA32 (Ser4, Ser8) from Bethyl Laboratories, catalog number A300-245A, polyclonal was run at 1:2000 concentration with a 30M citrate antigen retrieval (Leica ER1 AR9961). 2) Phospho-Histone H2A.X (Ser139) from Millipore Sigma, catalog number 05-636, clone JBW301 was run at 1:40,000 dilution with a 20M EDTA antigen retrieval (Leica ER2 AR9640).

Statistical Analysis

Data were analyzed and visualized using GraphPad Prism (Version 10.2.2, GraphPad Software, LLC). Statistical comparisons were made using either a two-tailed Student's t-test or a Mann-Whitney U test for two-group analyses. For multi-group comparisons, one-way ANOVA followed by Tukey's/any additional post-hoc test or a two-way mixed-model ANOVA was performed. Drug synergy was calculated using Bliss Independence Model in which a Bliss synergy score of more than 5 is considered synergistic (69, 70). Statistical significance was defined as $p<0.05$.

Study Approval

The study was approved by the Institutional Review Board (IRB) and IACUC committee at Dana-Farber Cancer Institute and Mayo Clinic Minnesota. All procedures were conducted in accordance with the Declaration of Helsinki.

Data Availability

All data utilized for analysis are included within this manuscript under “Supporting Data Values”. Requests for raw or analyzed data and materials related to this article that are not included in the manuscript within main text or supplemental materials will be reviewed by the respective institutions to determine if there are any intellectual property or confidentiality restrictions. Any shareable data or materials will be provided through a material transfer agreement.

Author Contributions

JPA, SA, GZ, ZL, GS, TW, JRC and AD designed the studies. JPA, SA, GZ, YH, DI, SM, KP, GZ, LJ, DY, MM, KG, XW conducted the studies. JPA, SA, GZ and AD wrote the manuscript and GIS and TW critically appraised it. JPA led the study with significant contributions from SA and GZ which defined the order of co-first authors. RK was the pathologist who read the IHC images. All authors reviewed and approved the final manuscript.

Acknowledgments

This work is supported by the Mayo Clinic and University of Iowa Lymphoma SPORE (P50 CA97274) and the Predolin Foundation. We thank Dana-Farber/Harvard Cancer Center in Boston, MA, for the use of the Specialized Histopathology Core, which provided histology and immunohistochemistry service. Dana-Farber/Harvard Cancer Center is supported in part by an NCI Cancer Center Support Grant # NIH 5 P30 CA06516. The work was also supported by the SENSHIN Medical Research Foundation and the Japan Society for the Promotion of Science (JSPS) Overseas Research Fellowships (to S.A.).

References

1. Técher H, Koundrioukoff S, Nicolas A, and Debatisse M. The impact of replication stress on replication dynamics and DNA damage in vertebrate cells. *Nat Rev Genet.* 2017;18(9):535-50.
2. Saxena S, and Zou L. Hallmarks of DNA replication stress. *Mol Cell.* 2022;82(12):2298-314.
3. Macheret M, and Halazonetis TD. Intragenic origins due to short G1 phases underlie oncogene-induced DNA replication stress. *Nature.* 2018;555(7694):112-6.
4. Hussmann JA, Ling J, Ravisankar P, Yan J, Cirincione A, Xu A, et al. Mapping the genetic landscape of DNA double-strand break repair. *Cell.* 2021;184(22):5653-69.e25.
5. Brambati A, Sacco O, Porcella S, Heyza J, Kareh M, Schmidt JC, et al. RHINO directs MMEJ to repair DNA breaks in mitosis. *Science.* 2023;381(6658):653-60.
6. Gelot C, Kovacs MT, Miron S, Mylne E, Haan A, Boeffard-Dosierre L, et al. Polθ is phosphorylated by PLK1 to repair double-strand breaks in mitosis. *Nature.* 2023;621(7978):415-22.
7. Srinivasan Seetha V, Dominguez-Sola D, Wang Lily C, Hyrien O, and Gautier J. Cdc45 Is a Critical Effector of Myc-Dependent DNA Replication Stress. *Cell Reports.* 2013;3(5):1629-39.
8. Al Zubaidi T, Gehrisch OHF, Genois M-M, Liu Q, Lu S, Kung J, et al. Targeting the DNA replication stress phenotype of KRAS mutant cancer cells. *Scientific Reports.* 2021;11(1):3656.
9. Xie M, Yen Y, Owonikoko TK, Ramalingam SS, Khuri FR, Curran WJ, et al. Bcl2 induces DNA replication stress by inhibiting ribonucleotide reductase. *Cancer Res.* 2014;74(1):212-23.
10. Ragu S, Matos-Rodrigues G, and Lopez BS. Replication Stress, DNA Damage, Inflammatory Cytokines and Innate Immune Response. *Genes (Basel).* 2020;11(4).
11. Menssen A, Epanchintsev A, Lodygin D, Rezaei N, Jung P, Verdoodt B, et al. c-MYC delays prometaphase by direct transactivation of MAD2 and BubR1: identification of mechanisms underlying c-MYC-induced DNA damage and chromosomal instability. *Cell Cycle.* 2007;6(3):339-52.
12. Barnum KJ, and O'Connell MJ. Cell cycle regulation by checkpoints. *Methods Mol Biol.* 2014;1170:29-40.
13. Zinkel S, Gross A, and Yang E. BCL2 family in DNA damage and cell cycle control. *Cell Death Differ.* 2006;13(8):1351-9.
14. Musgrove EA. Cyclins: roles in mitogenic signaling and oncogenic transformation. *Growth Factors.* 2006;24(1):13-9.
15. Tchakarska G, and Sola B. The double dealing of cyclin D1. *Cell Cycle.* 2020;19(2):163-78.
16. Terasawa M, Shinohara A, and Shinohara M. Canonical Non-Homologous End Joining in Mitosis Induces Genome Instability and Is Suppressed by M-phase-Specific Phosphorylation of XRCC4. *PLOS Genetics.* 2014;10(8):e1004563.
17. Zhao X, Wei C, Li J, Xing P, Li J, Zheng S, et al. Cell cycle-dependent control of homologous recombination. *Acta Biochim Biophys Sin (Shanghai).* 2017;49(8):655-68.
18. Montalto FI, and De Amicis F. Cyclin D1 in Cancer: A Molecular Connection for Cell Cycle Control, Adhesion and Invasion in Tumor and Stroma. *Cells.* 2020;9(12).
19. Bigoni R, Negrini M, Veronese ML, Cuneo A, Castoldi GL, and Croce CM. Characterization of t(11;14) translocation in mantle cell lymphoma by fluorescent in situ hybridization. *Oncogene.* 1996;13(4):797-802.

20. Yin CC, and Luthra R. Molecular detection of t(11;14)(q13;q32) in mantle cell lymphoma. *Methods Mol Biol.* 2013;999:211-6.
21. Garces S, Medeiros LJ, Marques-Piubelli ML, Coelho Siqueira SA, Miranda RN, Cuglievan B, et al. Cyclin D1 expression in Rosai-Dorfman disease: a near-constant finding that is not invariably associated with mitogen-activated protein kinase/extracellular signal-regulated kinase pathway activation. *Hum Pathol.* 2022;121:36-45.
22. Shanmugam V, Craig JW, Hornick JL, Morgan EA, Pinkus GS, and Pozdnyakova O. Cyclin D1 Is Expressed in Neoplastic Cells of Langerhans Cell Histiocytosis but Not Reactive Langerhans Cell Proliferations. *Am J Surg Pathol.* 2017;41(10):1390-6.
23. Terada Y, Inoshita S, Nakashima O, Kuwahara M, Sasaki S, and Marumo F. Regulation of cyclin D1 expression and cell cycle progression by mitogen-activated protein kinase cascade. *Kidney Int.* 1999;56(4):1258-61.
24. Milman T, Eiger-Moscovich M, Henry RK, Ida CM, Ruben M, Shields CL, et al. Cyclin D1 Expression and Molecular Genetic Findings in Periocular Histiocytoses and Neoplasms of Macrophage-Dendritic Cell Lineage. *Am J Ophthalmol.* 2022;242:36-51.
25. Joyce D, Albanese C, Steer J, Fu M, Bouzahzah B, and Pestell RG. NF-kappaB and cell-cycle regulation: the cyclin connection. *Cytokine & growth factor reviews.* 2001;12(1):73-90.
26. Mulloy R, Salinas S, Philips A, and Hipskind RA. Activation of cyclin D1 expression by the ERK5 cascade. *Oncogene.* 2003;22(35):5387-98.
27. Pawlonka J, Rak B, and Ambroziak U. The regulation of cyclin D promoters – review. *Cancer Treatment and Research Communications.* 2021;27:100338.
28. Müller H, Lukas J, Schneider A, Warthoe P, Bartek J, Eilers M, et al. Cyclin D1 expression is regulated by the retinoblastoma protein. *Proc Natl Acad Sci U S A.* 1994;91(8):2945-9.
29. Jirawatnotai S, Hu Y, Livingston DM, and Sicinski P. Proteomic identification of a direct role for cyclin d1 in DNA damage repair. *Cancer Res.* 2012;72(17):4289-93.
30. Shimura T, Ochiai Y, Noma N, Oikawa T, Sano Y, and Fukumoto M. Cyclin D1 overexpression perturbs DNA replication and induces replication-associated DNA double-strand breaks in acquired radioresistant cells. *Cell Cycle.* 2013;12(5):773-82.
31. Matsushime H, Ewen ME, Strom DK, Kato JY, Hanks SK, Roussel MF, et al. Identification and properties of an atypical catalytic subunit (p34PSK-J3/cdk4) for mammalian D type G1 cyclins. *Cell.* 1992;71(2):323-34.
32. Wang M, Sun L, Qian J, Han X, Zhang L, Lin P, et al. Cyclin D1 as a universally expressed mantle cell lymphoma-associated tumor antigen for immunotherapy. *Leukemia.* 2009;23(7):1320-8.
33. Vela-Chávez T, Adam P, Kremer M, Bink K, Bacon CM, Menon G, et al. Cyclin D1 positive diffuse large B-cell lymphoma is a post-germinal center-type lymphoma without alterations in the CCND1 gene locus. *Leuk Lymphoma.* 2011;52(3):458-66.
34. Navarro A, Beà S, Jares P, and Campo E. Molecular Pathogenesis of Mantle Cell Lymphoma. *Hematol Oncol Clin North Am.* 2020;34(5):795-807.
35. Tsegay PS, Lai Y, and Liu Y. Replication Stress and Consequential Instability of the Genome and Epigenome. *Molecules.* 2019;24(21).
36. Camacho E, Hernández L, Hernández S, Tort F, Bellosillo B, Beà S, et al. ATM gene inactivation in mantle cell lymphoma mainly occurs by truncating mutations and missense mutations involving the phosphatidylinositol-3 kinase domain and is associated with increasing numbers of chromosomal imbalances. *Blood.* 2002;99(1):238-44.

37. Schaffner C, Idler I, Stilgenbauer S, Döhner H, and Lichter P. Mantle cell lymphoma is characterized by inactivation of the ATM gene. *Proc Natl Acad Sci U S A.* 2000;97(6):2773-8.
38. AACR Project GENIE: Powering Precision Medicine through an International Consortium. *Cancer Discov.* 2017;7(8):818-31.
39. Liu S, Opiyo SO, Manthey K, Glanzer JG, Ashley AK, Amerin C, et al. Distinct roles for DNA-PK, ATM and ATR in RPA phosphorylation and checkpoint activation in response to replication stress. *Nucleic Acids Res.* 2012;40(21):10780-94.
40. Nakanishi K, Cavallo F, Brunet E, and Jasin M. Homologous recombination assay for interstrand cross-link repair. *Methods Mol Biol.* 2011;745:283-91.
41. Gunn A, and Stark JM. I-SceI-based assays to examine distinct repair outcomes of mammalian chromosomal double strand breaks. *Methods Mol Biol.* 2012;920:379-91.
42. Truong LN, Li Y, Shi LZ, Hwang PY, He J, Wang H, et al. Microhomology-mediated End Joining and Homologous Recombination share the initial end resection step to repair DNA double-strand breaks in mammalian cells. *Proc Natl Acad Sci U S A.* 2013;110(19):7720-5.
43. Williams ME, Swerdlow SH, and Meeker TC. Chromosome t(11;14)(q13;q32) breakpoints in centrocytic lymphoma are highly localized at the bcl-1 major translocation cluster. *Leukemia.* 1993;7(9):1437-40.
44. Sfeir A, Tijsterman M, and McVey M. Microhomology-Mediated End-Joining Chronicles: Tracing the Evolutionary Footprints of Genome Protection. *Annu Rev Cell Dev Biol.* 2024;40(1):195-218.
45. Ward TH, Cummings J, Dean E, Greystoke A, Hou JM, Backen A, et al. Biomarkers of apoptosis. *British Journal of Cancer.* 2008;99(6):841-6.
46. Nur EKA, Li TK, Zhang A, Qi H, Hars ES, and Liu LF. Single-stranded DNA induces ataxia telangiectasia mutant (ATM)/p53-dependent DNA damage and apoptotic signals. *The Journal of biological chemistry.* 2003;278(14):12475-81.
47. Abeykoon JP, Wu X, Nowakowski KE, Dasari S, Paludo J, Weroha SJ, et al. Salicylates enhance CRM1 inhibitor antitumor activity by induction of S-phase arrest and impairment of DNA-damage repair. *Blood.* 2021;137(4):513-23.
48. Vaitsiankova A, Burdova K, Sobol M, Gautam A, Benada O, Hanzlikova H, et al. PARP inhibition impedes the maturation of nascent DNA strands during DNA replication. *Nature Structural & Molecular Biology.* 2022;29(4):329-38.
49. Maya-Mendoza A, Moudry P, Merchut-Maya JM, Lee M, Strauss R, and Bartek J. High speed of fork progression induces DNA replication stress and genomic instability. *Nature.* 2018;559(7713):279-84.
50. Machacova Z, Chroma K, Lukac D, Protivankova I, and Moudry P. DNA polymerase α-primase facilitates PARP inhibitor-induced fork acceleration and protects BRCA1-deficient cells against ssDNA gaps. *Nat Commun.* 2024;15(1):7375.
51. Larson MH, Gilbert LA, Wang X, Lim WA, Weissman JS, and Qi LS. CRISPR interference (CRISPRi) for sequence-specific control of gene expression. *Nat Protoc.* 2013;8(11):2180-96.
52. Xiong Y, Wang Y, Li T, Yu X, Zeng Y, Xiao G, et al. A novel function for cyclin D1 as a transcriptional role in oncogenesis and tumor development by ChIP-Seq and RNA-Seq. *J Cancer.* 2021;12(17):5181-92.
53. Hill HA, Qi X, Jain P, Nomie K, Wang Y, Zhou S, et al. Genetic mutations and features of mantle cell lymphoma: a systematic review and meta-analysis. *Blood Adv.* 2020;4(13):2927-38.
54. Rahal EA, Henricksen LA, Li Y, Williams RS, Tainer JA, and Dixon K. ATM regulates Mre11-dependent DNA end-degradation and microhomology-mediated end joining. *Cell Cycle.* 2010;9(14):2866-77.

55. Riches LC, Trinidad AG, Hughes G, Jones GN, Hughes AM, Thomason AG, et al. Pharmacology of the ATM Inhibitor AZD0156: Potentiation of Irradiation and Olaparib Responses Preclinically. *Molecular Cancer Therapeutics.* 2020;19(1):13-25.
56. Ma MCJ, Tadros S, Bouska A, Heavican T, Yang H, Deng Q, et al. Subtype-specific and co-occurring genetic alterations in B-cell non-Hodgkin lymphoma. *Haematologica.* 2022;107(3):690-701.
57. Zhou J, Gelot C, Pantelidou C, Li A, Yücel H, Davis RE, et al. A first-in-class Polymerase Theta Inhibitor selectively targets Homologous-Recombination-Deficient Tumors. *Nat Cancer.* 2021;2(6):598-610.
58. Zatreanu D, Robinson HMR, Alkhatib O, Boursier M, Finch H, Geo L, et al. Polθ inhibitors elicit BRCA-gene synthetic lethality and target PARP inhibitor resistance. *Nature Communications.* 2021;12(1):3636.
59. Casimiro MC, Crosariol M, Loro E, Ertel A, Yu Z, Dampier W, et al. ChIP sequencing of cyclin D1 reveals a transcriptional role in chromosomal instability in mice. *J Clin Invest.* 2012;122(3):833-43.
60. Siraj AK, Parvathareddy SK, Annaiyappanaidu P, Ahmed SO, Siraj N, Tulbah A, et al. High Expression of Cyclin D1 is an Independent Marker for Favorable Prognosis in Middle Eastern Breast Cancer. *Onco Targets Ther.* 2021;14:3309-18.
61. Ogino S, Nosho K, Irahara N, Kure S, Shima K, Baba Y, et al. A cohort study of cyclin D1 expression and prognosis in 602 colon cancer cases. *Clin Cancer Res.* 2009;15(13):4431-8.
62. Gansauge S, Gansauge F, Ramadani M, Stobbe H, Rau B, Harada N, et al. Overexpression of cyclin D1 in human pancreatic carcinoma is associated with poor prognosis. *Cancer Res.* 1997;57(9):1634-7.
63. Shima N, Munroe RJ, and Schimenti JC. The mouse genomic instability mutation chaos1 is an allele of Polq that exhibits genetic interaction with Atm. *Molecular and cellular biology.* 2004;24(23):10381-9.
64. Belan O, Sebald M, Adamowicz M, Anand R, Vancevska A, Neves J, et al. POLQ seals post-replicative ssDNA gaps to maintain genome stability in BRCA-deficient cancer cells. *Molecular Cell.* 2022;82(24):4664-80.e9.
65. Schrempf A, Bernardo S, Arasa Verge EA, Ramirez Otero MA, Wilson J, Kirchhofer D, et al. POLθ processes ssDNA gaps and promotes replication fork progression in BRCA1-deficient cells. *Cell Rep.* 2022;41(9):111716.
66. Kwok M, Agathanggelou A, and Stankovic T. DNA damage response defects in hematologic malignancies: mechanistic insights and therapeutic strategies. *Blood.* 2024;143(21):2123-44.
67. M'Kacher R, Farace F, Bennaceur-Griscelli A, Violot D, Clausse B, Dossou J, et al. Blastoid mantle cell lymphoma: evidence for nonrandom cytogenetic abnormalities additional to t(11;14) and generation of a mouse model. *Cancer Genet Cytogenet.* 2003;143(1):32-8.
68. Wu X, Nowakowski KE, Abeykoon JP, Manske M, Stenson MJ, Timm MM, et al. MCIR1: A patient-derived mantle cell lymphoma line for discovering new treatments for ibrutinib resistance. *Eur J Haematol.* 2021;107(4):458-65.
69. Demidenko E, and Miller TW. Statistical determination of synergy based on Bliss definition of drugs independence. *PLoS One.* 2019;14(11):e0224137.
70. Zheng S, Wang W, Aldahdooh J, Malyutina A, Shadbahr T, Tanoli Z, et al. SynergyFinder Plus: Toward Better Interpretation and Annotation of Drug Combination Screening Datasets. *Genomics, Proteomics & Bioinformatics.* 2022;20(3):587-96.

Figure Legends

Figure 1: Cyclin D1 overexpression increases DNA damage, replication stress, and MMEJ-mediated DNA damage repair. (A) Replication stress assessed via pRPA S33 foci using immunofluorescence microscopy in cyclin D1 overexpressed U2OS cells (experiments were done in triplicates, p-value was calculated using one-way ANOVA with Tukey's post-hoc test). **(B** and **C)** DNA damage was assessed via γ-H2AX in the corresponding cells (experiments were done in triplicates, p-value was calculated using one-way ANOVA with Tukey's post-hoc test). **(D)** DNA double-strand break repair pathway assessment in cyclin D1 overexpressed reporter cells (experiments were done in quadruplicates, p-value was calculated using t-test). **(E** and **F)** Assessment of POLΘ foci in cyclin D1 overexpressed U2OS cells in which endogenous POLΘ is tagged via V5 epitope (experiments were done in triplicates, p-value was calculated using one-way ANOVA with Tukey's post-hoc test). EV: empty vector; OE: overexpressed; MMEJ: microhomology-mediated end-joining; NHEJ: non-homologous end-joining; HR: homologous recombination; * $p<0.05$; ** $p<0.01$; *** $p<0.001$; ****$p <0.0001$. Error bars represent Standard Error of the Means (SEM).

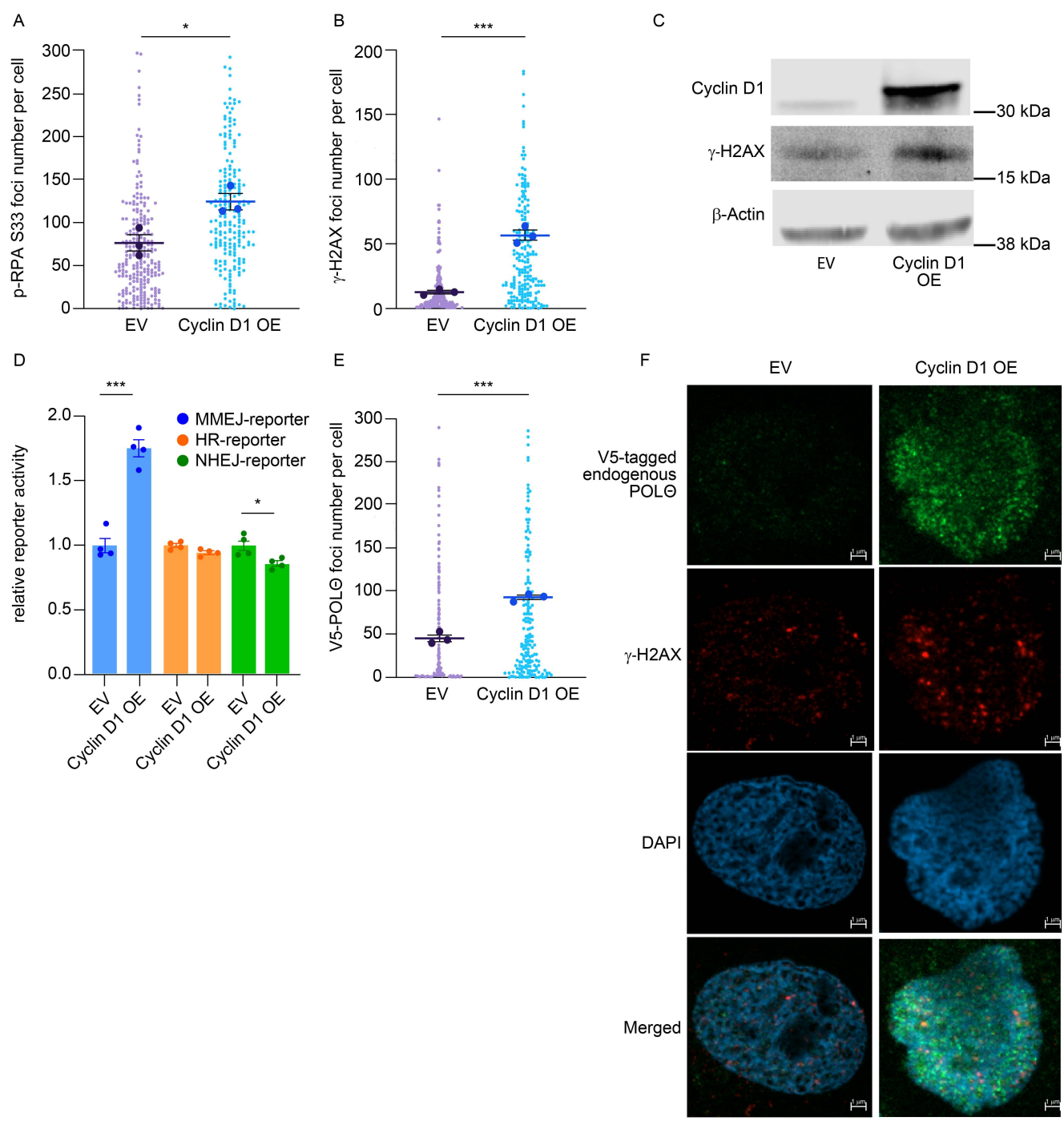
A
p-RPA S33 foci number per cell
*
EV
Cyclin D1 OE
B
γ-H2AX foci number per cell
***
EV
Cyclin D1 OE
C
Cyclin D1
γ-H2AX
β-Actin
30 kDa
15 kDa
38 kDa
EV
Cyclin D1 OE
D
relative reporter activity
***
*
MMEJ-reporter
HR-reporter
NHEJ-reporter
EV
Cyclin D1 OE
E
V5-POLΘ foci number per cell
***
EV
Cyclin D1 OE
F
EV
Cyclin D1 OE
V5-tagged endogenous POLΘ
γ-H2AX
DAPI
Merged

Figure 1

Figure 2: Mantle cell lymphoma cells rely on POLΘ and MMEJ mediated double-strand break repair to repair mitotic DNA double-strand breaks and to mitigate detrimental replication stress. (A) Assessment of DNA damage as the mantle cell lymphoma cell traverse through the different phases of the cell cycle in POLΘ deficient and proficient conditions. **(B)** Assessment of replication stress through pRPA S33 foci in unsynchronized and mitotic synchronized cells based on POLΘ proficiency (experiments were done in triplicates, p-value was calculated using one-way ANOVA with Tukey's post-hoc test). **(C** and **D)** Assessment of mitotic DNA damage in POLΘ proficient and deficient MCL cells via γ-H2AX foci and comet assay, respectively (experiments were done in triplicates, p-value was calculated using one-way ANOVA with Tukey's post-hoc test). **(E)** Assessment of apoptotic marker (cleaved PARP) and DNA damage (γ-H2AX) in POLΘ proficient and deficient mitotically synchronized (validated by cyclin B1 expression) and unsynchronized MCL cells. **(F** and **G)** Assessment of chromosomal stability (red arrows showing double minute chromosomes and blue arrow showing a dicentric chromosome) in POLΘ deficient and proficient MCL cells (experiments were done in triplicates, p-value was calculated using one-way ANOVA with Tukey's post-hoc test). **(H** and **I)** Prevalence of single-stranded DNA in MCL cells with and without POLΘ assessed through DNA fiber S1 nuclease assay (experiments were done in quadruplicates, p-value was calculated using one-way ANOVA with Tukey's post-hoc test). sg: single-guide; NT: non-target; OE: overexpressed; S1: S1 nuclease; ns: not significant; MMEJ: microhomology mediated end-joining; * $p<0.05$; ** $p<0.01$; *** $p<0.001$; **** $p<0.0001$. Error bars represent SEM.

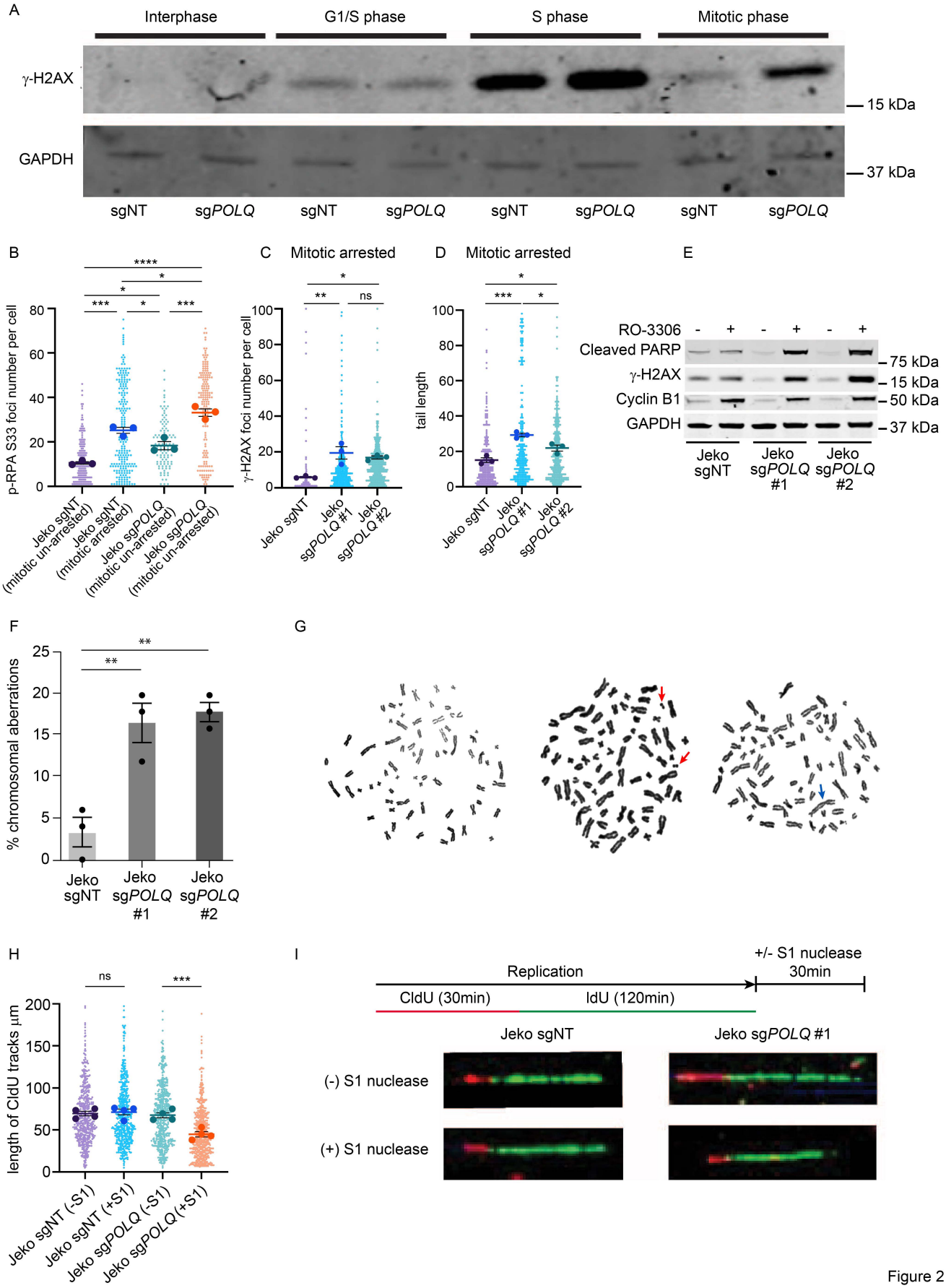
A
Interphase
G1/S phase
S phase
Mitotic phase
γ-H2AX
15 kDa
GAPDH
37 kDa
sgNT
sgPOLQ
B
p-RPA S33 foci number per cell
Jeko sgNT (mitotic un-arrested)
Jeko sgNT (mitotic arrested)
Jeko sgPOLQ (mitotic un-arrested)
Jeko sgPOLQ (mitotic un-arrested)
C
Mitotic arrested
γ-H2AX foci number per cell
ns
Jeko sgNT
Jeko sgPOLQ #1
Jeko sgPOLQ #2
D
Mitotic arrested
tail length
E
RO-3306
Cleaved PARP
γ-H2AX
Cyclin B1
GAPDH
75 kDa
15 kDa
50 kDa
37 kDa
Jeko sgNT
Jeko sgPOLQ #1
Jeko sgPOLQ #2
F
% chromosomal aberrations
Jeko sgNT
Jeko sgPOLQ #1
Jeko sgPOLQ #2
G
H
length of CldU tracks µm
ns
Jeko sgNT (-S1)
Jeko sgNT (+S1)
Jeko sgPOLQ (-S1)
Jeko sgPOLQ(+S1)
I
Replication
+/- S1 nuclease 30min
CldU (30min)
IdU (120min)
Jeko sgNT
Jeko sgPOLQ #1
(-) S1 nuclease
(+) S1 nuclease

Figure 2

Figure 3: Cyclin D1 overexpression specifically increases the expression of *POLQ* through binding to the *POLQ* promoter, which leads to an increased MMEJ-mediated DNA damage repair. (A) Assessment of *POLQ* expression and DNA damage (γ-H2AX) in MCL cells (Jeko) when cyclin D1 expression is decreased through CRISPRi technology. **(B)** Quantification of *POLQ* and *CCND1* transcription in Jeko cells with decreased cyclin D1 expression (experiments were done in quadruplicates, p-value is calculated using t-test). **(C)** Assessment of MMEJ mediated DNA damage repair in Jeko cells with decreased cyclin D1 expression (experiments were done in quadruplicates, p-value is calculated using t-test). **(D)** Assessment of sensitivity to POLΘ inhibition (ART558) in Jeko cells with decreased cyclin D1 expression (experiments were done in triplicates, p-value is calculated using t-test). **(E)** Assessment of *POLQ* expression with lentiviral mediated cyclin D1 overexpression in multiple non-Hodgkin lymphoma cell lines belonging to T-cell lymphoma (SR786 and Karpas 299), and diffuse large B-cell lymphoma (Ly1, Ly19, DHL6) (experiments were done in triplicates, p-value is calculated using t-test). **(F)** Evaluating cyclin D1 binding to *POLQ* promoter region through chromatin immunoprecipitation in HA tagged cyclin D1 overexpressed MCL cells (Jeko cells with endogenous cyclin D1 expression is stably decreased) (experiments were done in triplicates, p-value was calculated using one-way ANOVA with Tukey's post-hoc test). **(G)** Assessment of the transcriptional activity of the *POLQ* promoter using a luciferase assay in cells with cyclin D1 overexpression (experiments were done in triplicates, p-value was calculated using one-way ANOVA with Tukey's post-hoc test). sg: single-guide; NT: non-target; OE: overexpressed; * $p<0.05$; ** $p<0.01$; *** $p<0.001$; ****$p<0.0001$. Error bars represent SEM.

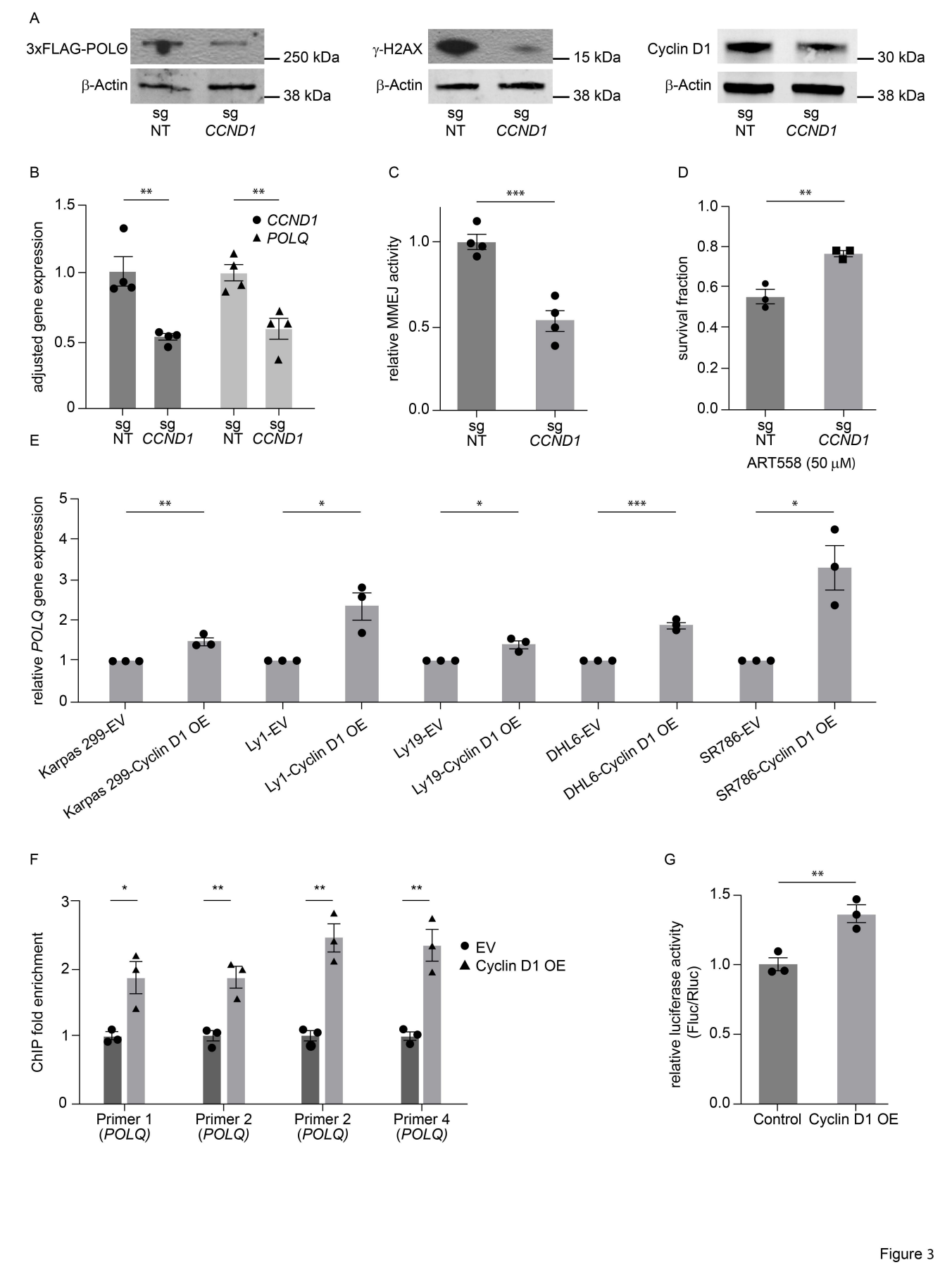
A
3xFLAG-POLΘ
250 kDa
β-Actin
38 kDa
sg NT
sg CCND1
γ-H2AX
15 kDa
β-Actin
38 kDa
sg NT
sg CCND1
Cyclin D1
30 kDa
β-Actin
38 kDa
sg NT
sg CCND1
B
adjusted gene expression
CCND1
POLQ
sg NT
sg CCND1
sg NT
sg CCND1
C
relative MMEJ activity
sg NT
sg CCND1
D
survival fraction
sg NT
sg CCND1
ART558 (50 μM)
E
relative POLQ gene expression
Karpas 299-EV
Karpas 299-Cyclin D1 OE
Ly1-EV
Ly1-Cyclin D1 OE
Ly19-EV
Ly19-Cyclin D1 OE
DHL6-EV
DHL6-Cyclin D1 OE
SR786-EV
SR786-Cyclin D1 OE
F
ChIP fold enrichment
EV
Cyclin D1 OE
Primer 1 (POLQ)
Primer 2 (POLQ)
Primer 2 (POLQ)
Primer 4 (POLQ)
G
relative luciferase activity (Fluc/Rluc)
Control
Cyclin D1 OE

Figure 3

Figure 4: Concurrent deficiency in ATM with cyclin D1 overexpression augments replication stress, mitotic DNA damage, and MMEJ mediated DNA damage repair. (A) Replication stress assessment via pRPA S33 foci and **(B)** DNA damage assessment via γ-H2AX in cyclin D1 overexpressed and ATM-deficient cells U2OS cells (experiments were done in triplicates, p-value is calculated using one-way ANOVA with Tukey's post-hoc test). **(C)** Assessment of DNA damage via γ-H2AX in mitotically synchronized POLΘ deficient Jeko cells with ATM inhibition (AZD0156 1μM) after mitotic synchronization using RO-3306 (experiments were done in triplicates, p-value is calculated using one-way ANOVA with Tukey's post-hoc test). **(D)** Assessment of replication stress through a validated marker (phosphorylated CHK1) in POLΘ proficient and deficient Jeko cells with and without ATM inhibition in unsynchronized and mitotically synchronized cells using RO-3306 (lanes were run in the same gel but displayed separately to facilitate comparison within the unsynchronized and mitotic arrested groups). **(E)** MMEJ mediated DNA double-strand break repair assessment through a validated reporter in cyclin D1 overexpressed and ATM-deficient background in U2OS reporter cells (experiments were done in quadruplicates, p-value is calculated using one-way ANOVA with Tukey's post-hoc test). **(F)** Assessment of *POLQ* mRNA expression in isogeneic Mino cell line with and without ATM deficiency (experiments were done in quintuplets and p-value is calculated using t-test)**.** sg: single-guide; EV: empty vector; KO: knock-out; NT: non-target; OE: overexpressed; ns: not significant; ATMi: ATM inhibitor; MMEJ: microhomology mediated end-joining; * $p<0.05$; ** $p<0.01$; *** $p<0.001$; ****$p<0.0001$. Error bars represent SEM.

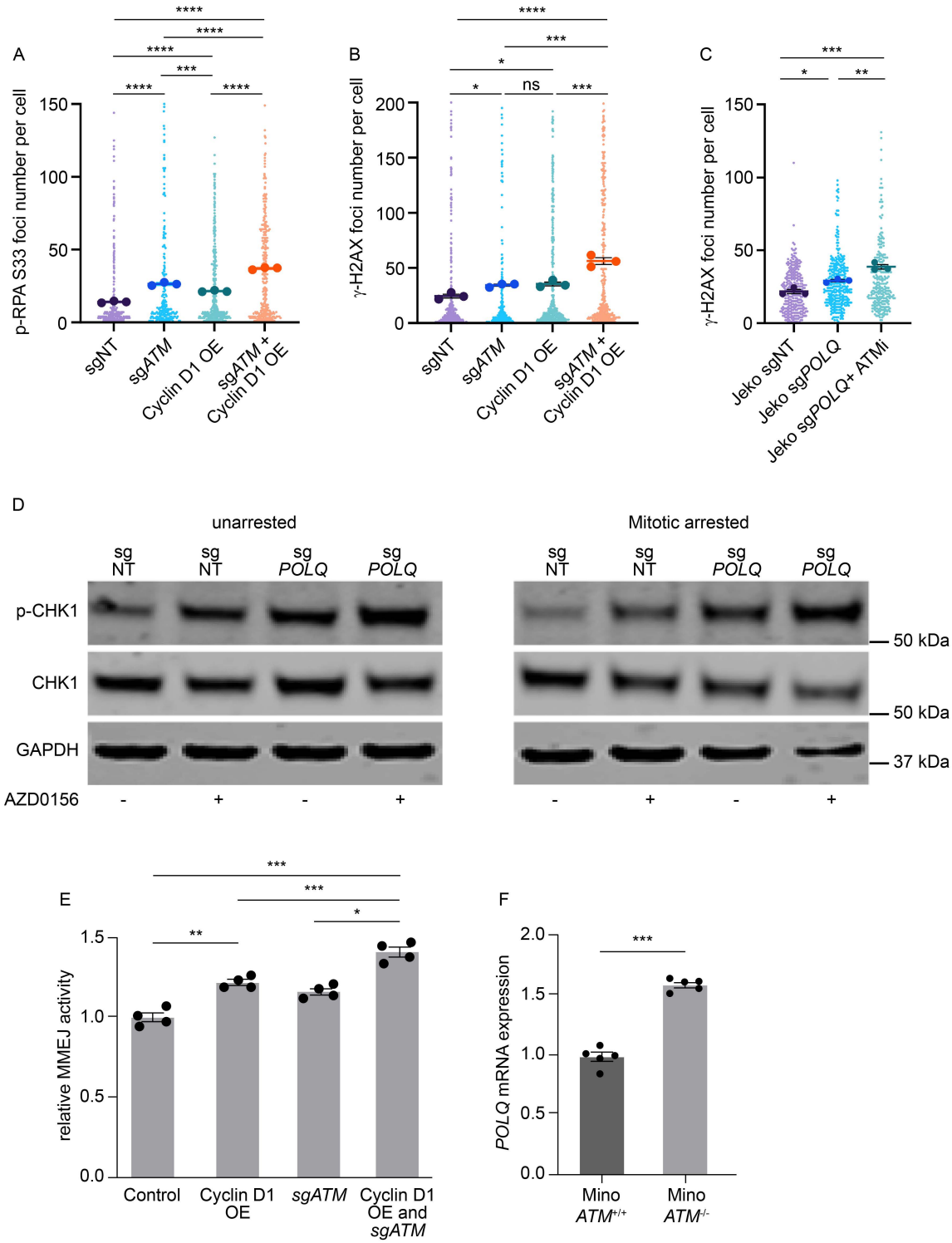
A
p-RPA S33 foci number per cell
sgNT
sgATM
Cyclin D1 OE
sgATM + Cyclin D1 OE
B
γ-H2AX foci number per cell
ns
C
γ-H2AX foci number per cell
Jeko sgNT
Jeko sgPOLQ
Jeko sgPOLQ+ ATMi
D
unarrested
Mitotic arrested
sg NT
sg POLQ
p-CHK1
CHK1
GAPDH
AZD0156
50 kDa
37 kDa
E
relative MMEJ activity
Control
Cyclin D1 OE
sgATM
Cyclin D1 OE and sgATM
F
POLQ mRNA expression
Mino ATM+/+
Mino ATM-/-

Figure 4

Figure 5: POLΘ protein expression is further increased by ATM deficiency in cyclin D1-overexpressing cells. (A) Evaluating POLΘ expression (endogenous *POLQ* tagged with V5 epitope) in U2OS cells with cyclin D1 overexpressed and ATM-deficient setting. **(B** and **C)** Assessment of γ-H2AX foci and POLΘ foci in cyclin D1 overexpressed and ATM-deficient background in U2OS cells (experiments were done in triplicates, p-value was calculated using one-way ANOVA with Tukey's post-hoc test). sg: single-guide; EV: empty vector; KO: knock-out; NT: non-target; OE: overexpressed; ns: not significant; * $p<0.05$; ** $p<0.01$; *** $p<0.001$; **** $p<0.0001$. Error bars represent SEM.

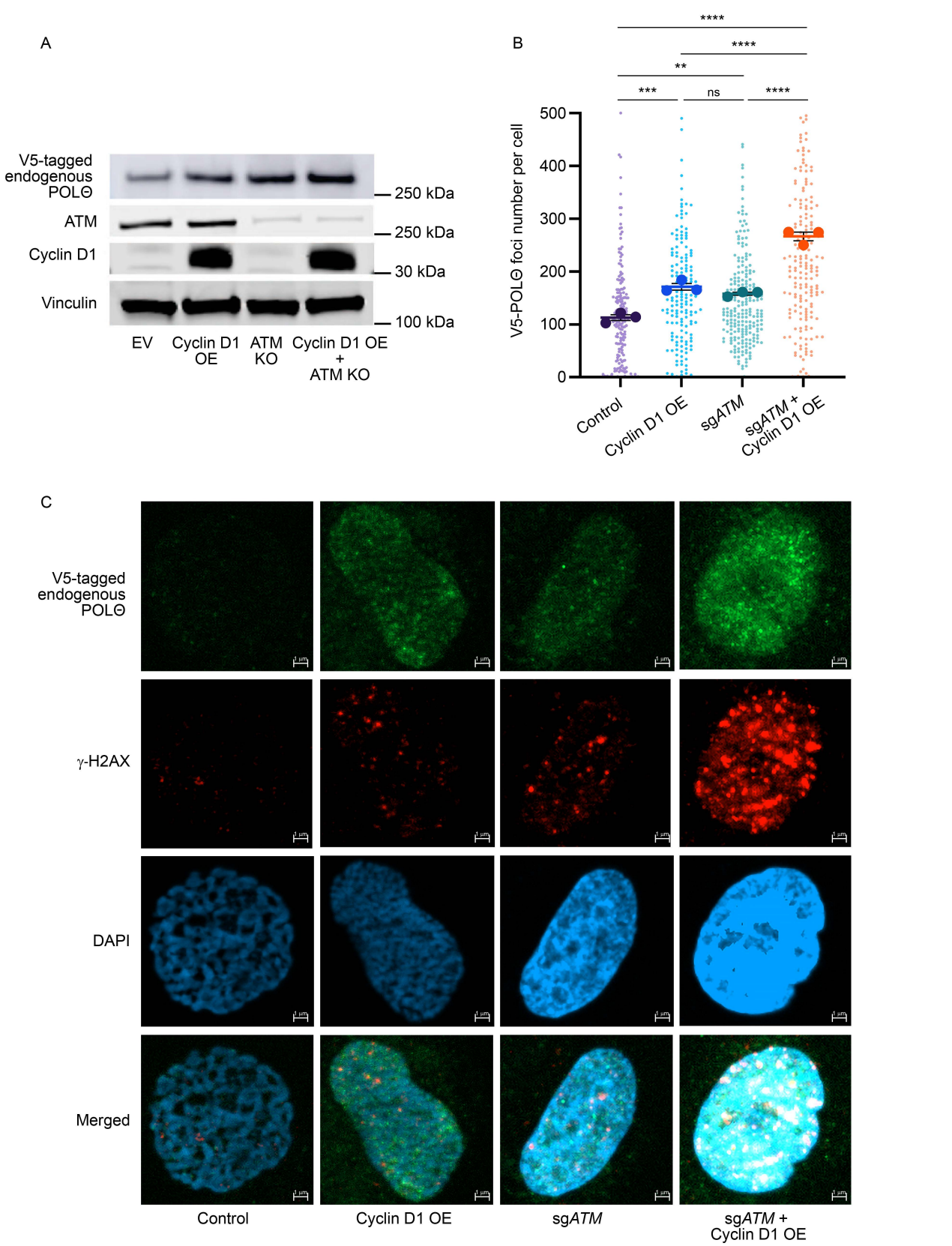
A
V5-tagged endogenous POLΘ
ATM
Cyclin D1
Vinculin
250 kDa
250 kDa
30 kDa
100 kDa
EV
Cyclin D1 OE
ATM KO
Cyclin D1 OE + ATM KO
B
****
****
**
***
ns
****
V5-POLΘ foci number per cell
500
400
300
200
100
0
Control
Cyclin D1 OE
sgATM
sgATM + Cyclin D1 OE
C
V5-tagged endogenous POLΘ
γ-H2AX
DAPI
Merged
Control
Cyclin D1 OE
sgATM
sgATM + Cyclin D1 OE

Figure 5

Figure 6: POLΘ inhibition induces a significant antitumor effect in MCL, and is augmented by concurrent ATM deficiency. (A) Assessment of rate of proliferation and viability using a competitive assay in two MCL cell lines (Jeko-ATM proficient and UPN2-ATM deficient) with genetic depletion of *POLQ* (experiments were done in triplicates). **(B** and **C)** Cell viability assessment on MCL cell lines using two POLΘ inhibitors, ART558 and novobiocin (NVB) (experiments were done in triplicates). **(D)** Assessment of antiproliferative and apoptotic effect with *POLQ* and *ATM* genetic depletion using Jeko cell line (experiments were done in quadruplicates, p-value was calculated by two-way mixed-model ANOVA). **(E)** Graph illustrating the sensitivity to POLΘ inhibition by NVB in ATM-deficient and proficient Mino cells (experiments were done in triplicates). **(F** and **G)** Assessment of cell killing and synergy (Bliss synergy score 72.91) in Jeko cells with concurrent inhibition of ATM using AZD0156 and POLΘ with ART558 (experiments were done in triplicates). **(H)** Genetically depleted *POLQ* in Jeko cells being treated with AZD0156 to assess cell killing in *POLQ* deficient and proficient background (experiments were done in triplicates). sg: single-guide; EV: empty vector; KO: knock-out; NT: non-target; OE: overexpressed; * $p<0.05$; ** $p<0.01$; *** $p<0.001$; ****$p <0.0001$. Error bars represent the standard deviation.

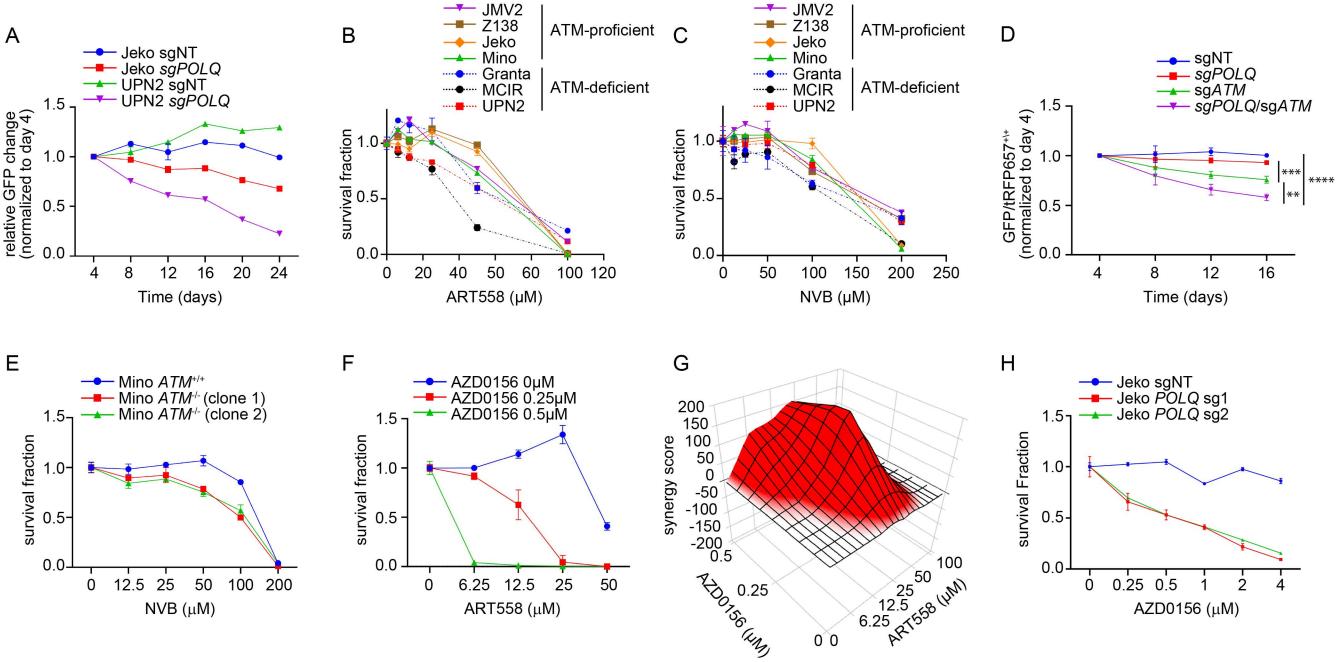
A
Jeko sgNT
Jeko sgPOLQ
UPN2 sgNT
UPN2 sgPOLQ
relative GFP change (normalized to day 4)
Time (days)
B
JMV2
Z138
Jeko
Mino
Granta
MCIR
UPN2
ATM-proficient
ATM-deficient
survival fraction
ART558 (μM)
C
NVB (μM)
D
sgNT
sgPOLQ
sgATM
sgPOLQ/sgATM
GFP/tRFP657+/+ (normalized to day 4)
***
**
****
E
Mino ATM+/+
Mino ATM-/- (clone 1)
Mino ATM-/- (clone 2)
F
AZD0156 0μM
AZD0156 0.25μM
AZD0156 0.5μM
G
synergy score
AZD0156 (μM)
ART558 (μM)
H
Jeko sgNT
Jeko POLQ sg1
Jeko POLQ sg2
survival Fraction
AZD0156 (μM)

Figure 6

Figure 7: POLΘ depletion induces significant antitumor effect in vivo MCL model, and the effect is augmented with ATM deficiency. (A) Using immunodeficient mice, ATM deficient and proficient isogeneic Mino cells were engrafted and treated with novobiocin (NVB) or vehicle (PBS). Each treatment group had eight mice in total (four females and four males, p-value was calculated by two-way mixed-model ANOVA). The antitumor effect was assessed through tumor measurements. **(B)** Overall survival of mice carrying MCL tumors with respective genotypes treated with NVB or vehicle (survival analysis was done using four mice per group). **(C** and **D)** Assessment of replication stress marker p-RPA S4/S8 via immunohistochemistry (IHC) in MCL tumor tissue following treatment with either NVB or vehicle (four mice [1:1 male and female] per group, p-value was calculated using one-way ANOVA with Tukey's post-hoc test). **(E** and **F)** Assessment of DNA damage marker γ-H2AX in respective tumor types following treatment with either NVB or vehicle (four mice [1:1 male and female] per group, p-value was calculated using one-way ANOVA with Tukey's post-hoc test). PBS: phosphate buffered saline; NVB: novobiocin; * $p<0.05$; ** $p<0.01$; *** $p<0.001$; ****$p<0.0001$. Error bars represent SEM.

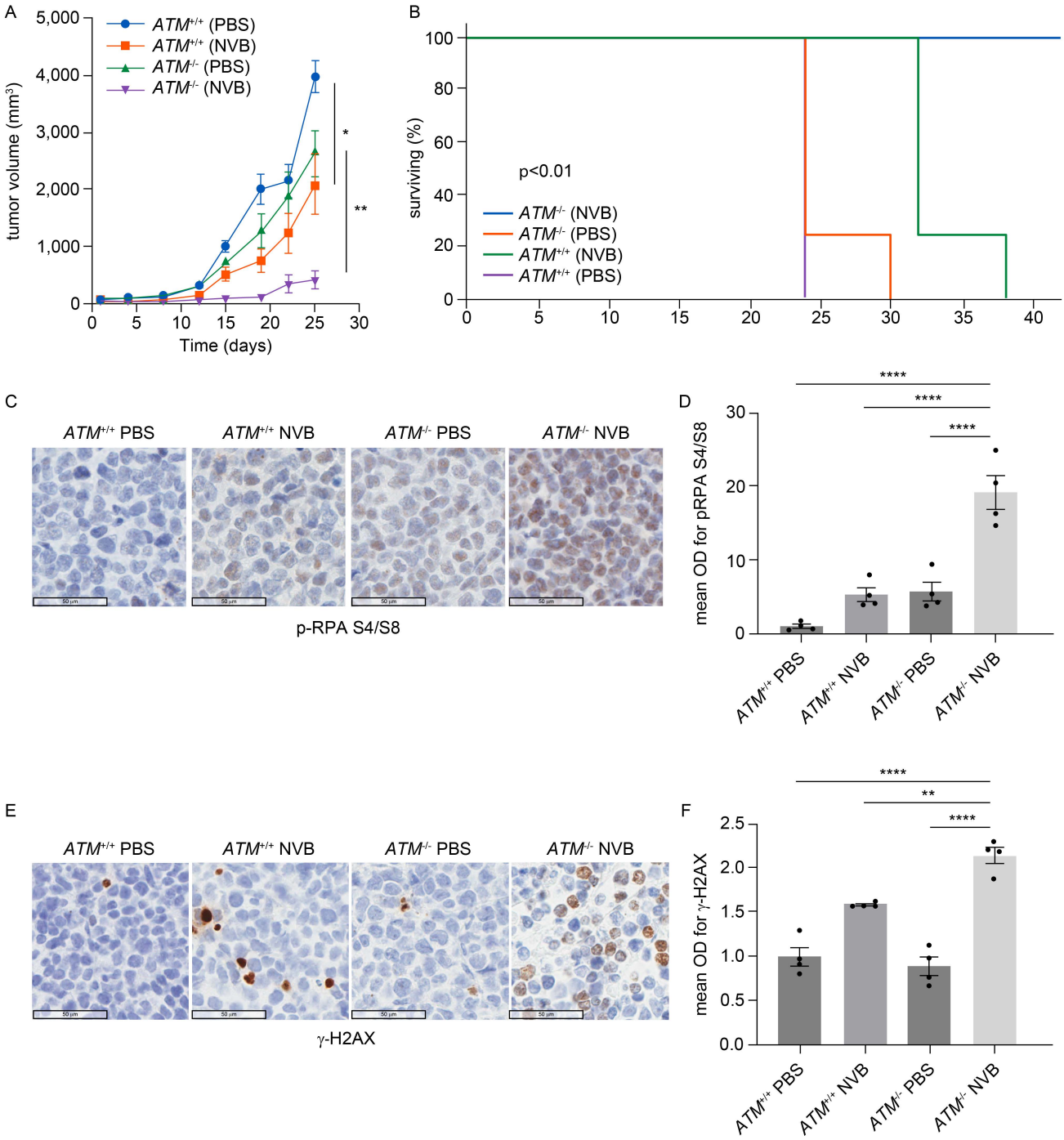
A
tumor volume (mm3)
Time (days)
ATM+/+ (PBS)
ATM+/+ (NVB)
ATM-/- (PBS)
ATM-/- (NVB)
*
**
B
surviving (%)
p<0.01
ATM-/- (NVB)
ATM-/- (PBS)
ATM+/+ (NVB)
ATM+/+ (PBS)
C
ATM+/+ PBS
ATM+/+ NVB
ATM-/- PBS
ATM-/- NVB
p-RPA S4/S8
D
mean OD for pRPA S4/S8
****
****
****
E
ATM+/+ PBS
ATM+/+ NVB
ATM-/- PBS
ATM-/- NVB
γ-H2AX
F
mean OD for γ-H2AX
****
**
****

Figure 7

Figure 8: *POLQ* is overexpressed in MCL compared to other NHL, and its inhibition showed an antitumor effect in primary tumor cells. (A) A representative figure of cyclin D1 expression was assessed through IHC in MCL compared to other non-Hodgkin lymphoma (400x magnification). **(B)** Assessment of *POLQ* expression in MCL compared to other types of non-Hodgkin lymphoma primary cells (n=8 FL, n=8 DLBCL, n=17 CLL/SLL, n=11 MZL, n=27 MCL, p value is calculated by one-way ANOVA with Tukey's post-hoc test). **(C** and **D)** POLΘ inhibition by ART558 causes a significant antitumor effect in primary MCL patient samples with increased antitumor effect seen in ATM deficient compared to ATM proficient primary MCL cells (experiments were done in triplicates, p-value was calculated by t-test). **(E** and **F)** Concurrent inhibition of ATM and POLΘ increases the antitumor effect compared to POLΘ inhibition alone in primary MCL cells (experiments were done in triplicates). MCL: mantle cell lymphoma; FL: follicular lymphoma; DLBCL: diffuse large B-cell lymphoma; MZL: marginal zone lymphoma; PTCL: primary cutaneous T-cell lymphoma; CLL/SLL: chronic lymphocytic leukemia/small lymphocytic lymphoma; H&E: hematoxylin and eosin stain; Pt: patient. Error bars represent SEM on Figure B and D and the standard deviation on Figure C, E and F. Red triangles in Figure B represent ATM deficient MCL primary samples. * $p<0.05$; ** $p<0.01$; *** $p<0.001$; **** $p<0.0001$.

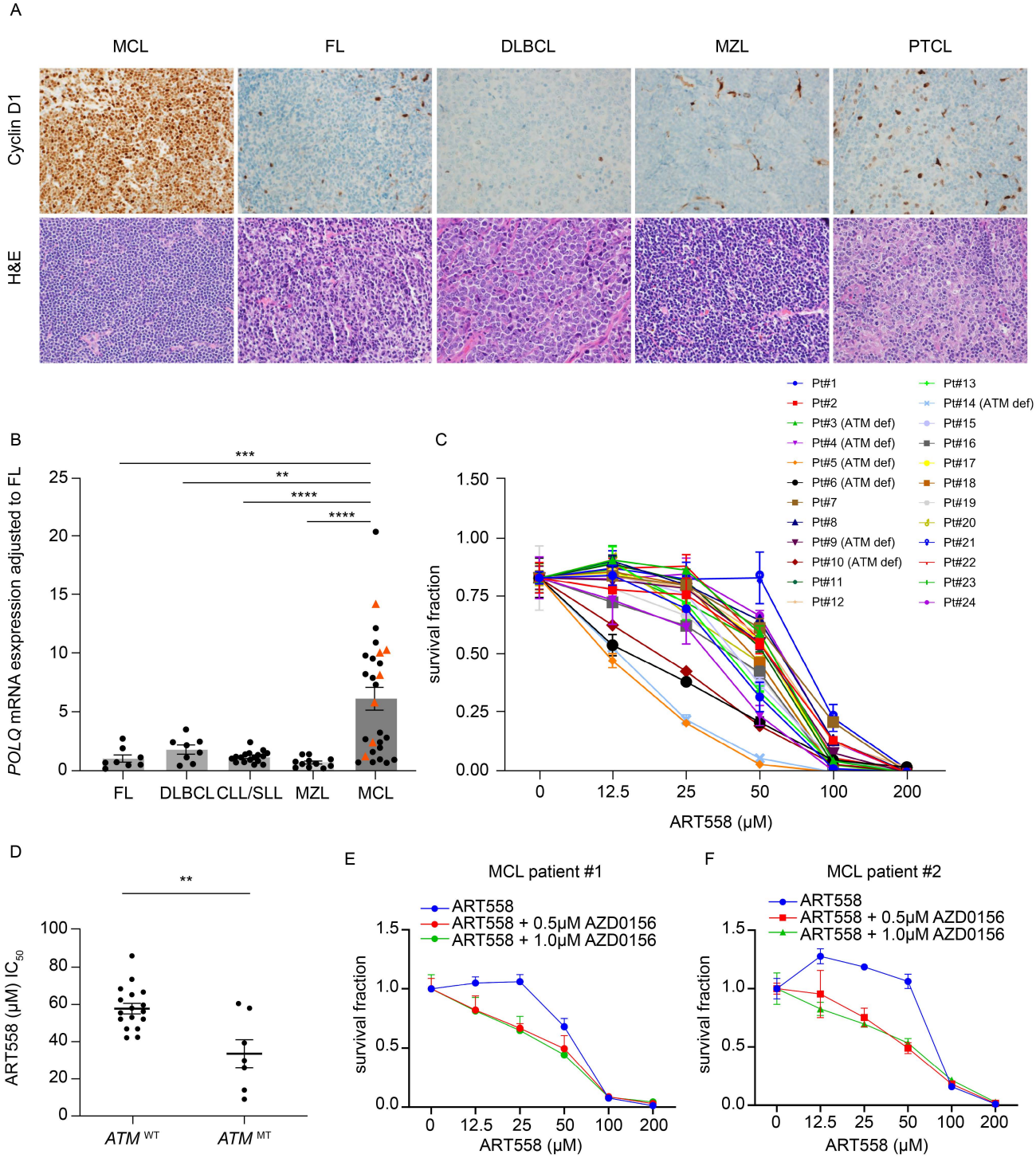
A
MCL
FL
DLBCL
MZL
PTCL
Cyclin D1
H&E
B
POLQ mRNA esxpression adjusted to FL
***
**
****
****
FL
DLBCL
CLL/SLL
MZL
MCL
C
survival fraction
ART558 (μM)
Pt#1
Pt#2
Pt#3 (ATM def)
Pt#4 (ATM def)
Pt#5 (ATM def)
Pt#6 (ATM def)
Pt#7
Pt#8
Pt#9 (ATM def)
Pt#10 (ATM def)
Pt#11
Pt#12
Pt#13
Pt#14 (ATM def)
Pt#15
Pt#16
Pt#17
Pt#18
Pt#19
Pt#20
Pt#21
Pt#22
Pt#23
Pt#24
D
ART558 (μM) IC50
**
ATM WT
ATM MT
E
MCL patient #1
ART558
ART558 + 0.5μM AZD0156
ART558 + 1.0μM AZD0156
survival fraction
ART558 (μM)
F
MCL patient #2
ART558
ART558 + 0.5μM AZD0156
ART558 + 1.0μM AZD0156
survival fraction
ART558 (μM)

Figure 8

Supplemental Figure 1: (A) Assessment of cell proliferation with cyclin D1 overexpression in U2OS (experiments were done in triplicates). **(B)** Immunoblot depicting cyclin D1 overexpression in reporter cells used to assess DNA double-strand break repair pathways with respective genetic alterations (Figure 1D). **(C-E)** valuation of V5 tagged to N terminus of endogenous POLΘ in U2OS cell line (experiments were done in triplicates and , p value was calculated by t-test). EV: empty vector; OE: overexpressed; sg: single guide RNA; MMEJ: microhomology mediated end-joining; HR: homologous recombination; NHEJ: non-homologous end-joining; ****p <0.0001. Error bars represent SEM.

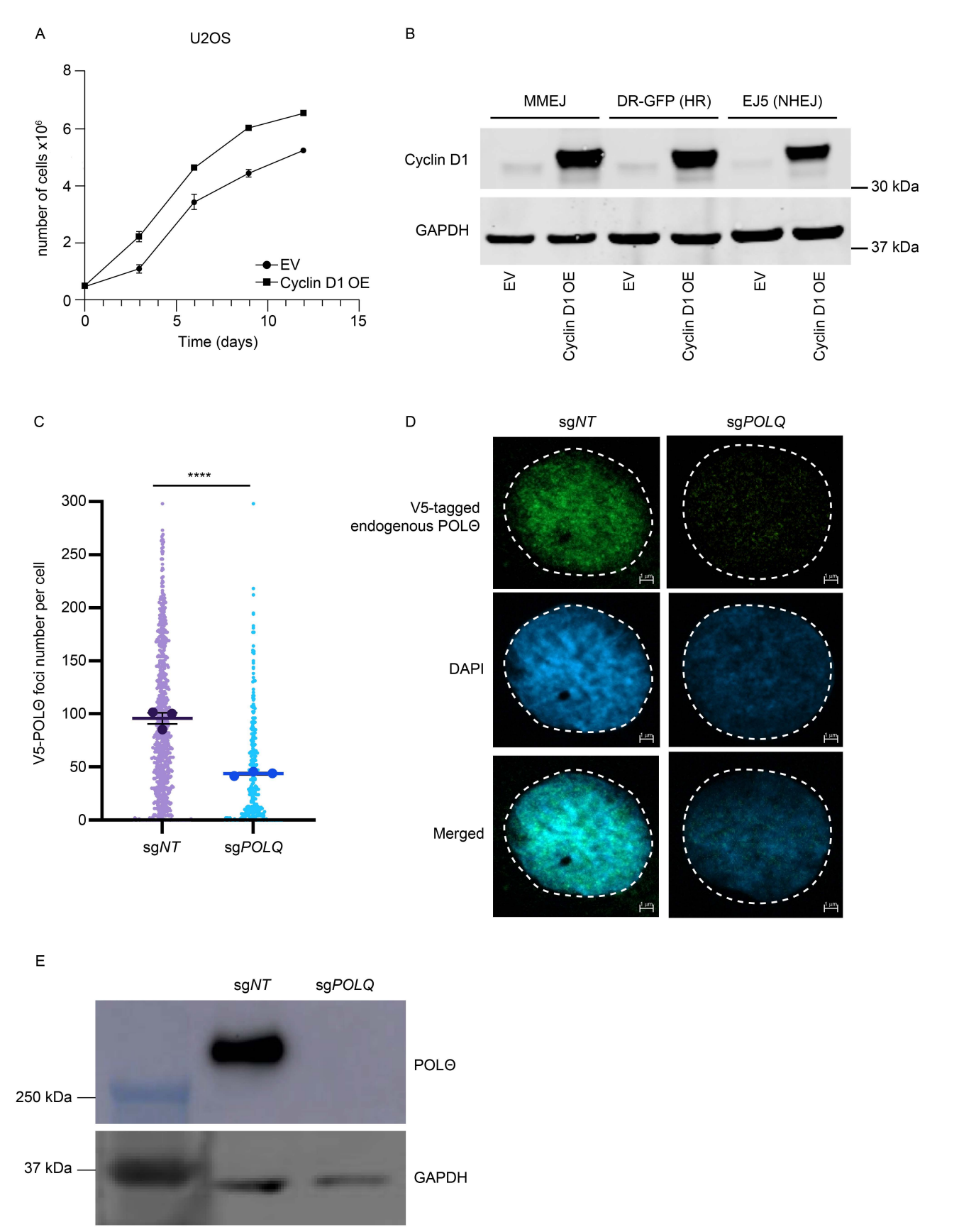

Supplemental Figure 1

Supplemental Figure 2: (A) Immunoblot depicting POLΘ in POLΘ depleted isogeneic Jeko cells. **(B)** Cell cycle analysis using propidium iodide to assess G_1, S and M-phase arrest on Jeko cells. **(C)** Cell cycle analysis using propidium iodide to assess M-phase arrest. **(D** and **E)** Antitumor effect of ATR and PARP inhibition in POLΘ–proficient and deficient backgrounds in Jeko cells (experiments were done in triplicates). sg: single-guide; NT: non-target. Error bars represent the standard deviation.

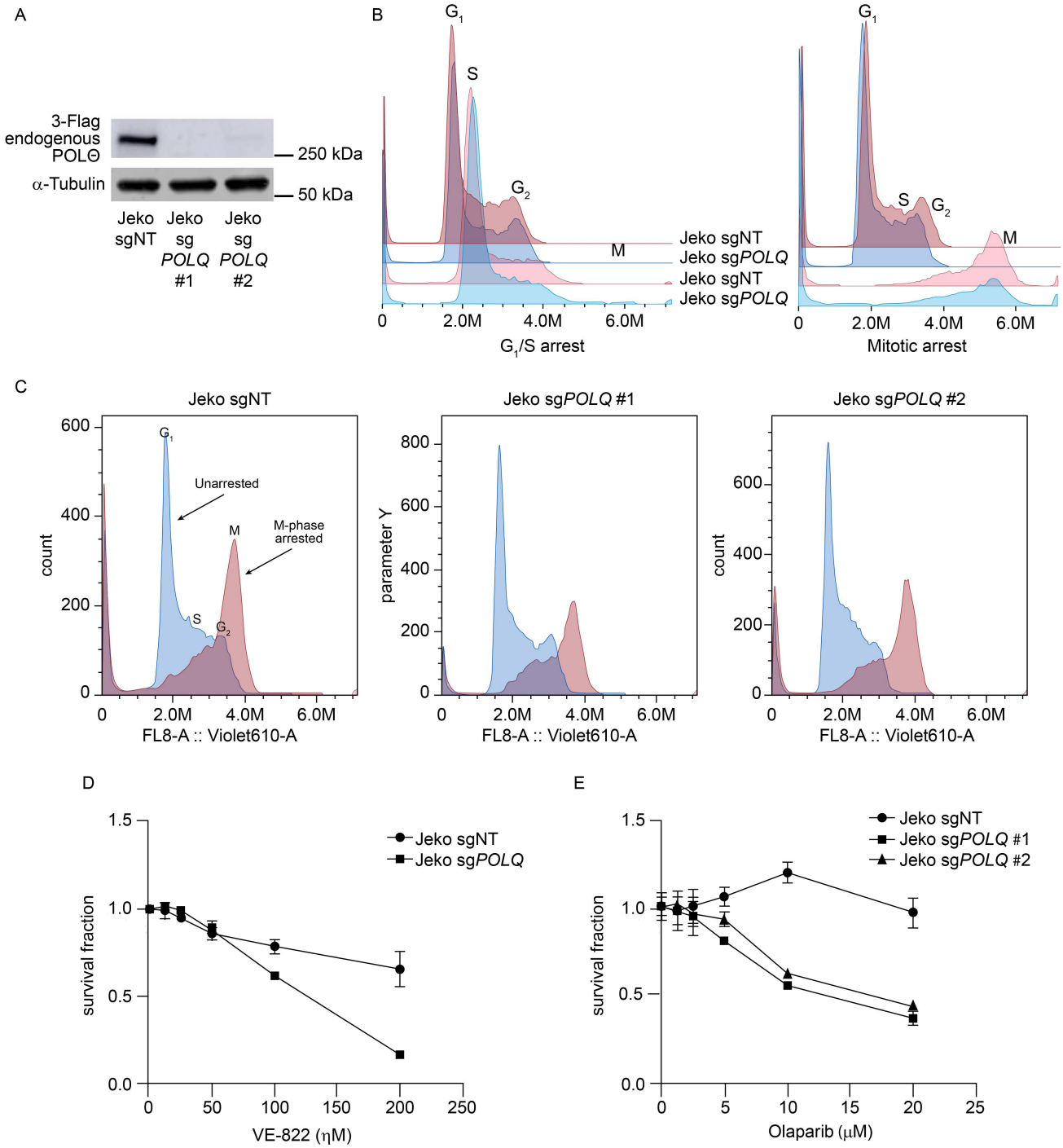

Supplemental Figure 2

Supplemental Figure 3: (A) Cell cycle assessment with CRISPRi-mediated decreased expression of cyclin D1 in Jeko cells (experiments were done in triplicates). **(B)** Immunoblot depicting Jeko cells used for Figure 3F in which CRISPRi induced decreased expression of endogenous cyclin D1 and overexpression of HA-tagged ectopic cyclin D1. **(C)** Immunoblot assessing HA-tagged ectopic cyclin D1 in U2OS cells used for experiments in supplemental Figure 3G. **(D** and **E)** Assessment of *ATM* mRNA in U2OS cells with and without cyclin D1 overexpression (D, experiments were done in sextuplicate, p value was calculated by t-test) and in Jeko cells with and without decreased expression of cyclin D1 (E, experiments were done in quintuplicate, p value was calculated by t-test). **(F)** Assessment of the enrichment of *ATM* promoter region through chromatin immunoprecipitation in HA-tagged cyclin D1 overexpressed Jeko cells with CRISPRi mediated decreased expression of endogenous cyclin D1 (experiments were done in triplicates). **(G)** Evaluating cyclin D1 binding to *POLQ* promoter region through chromatin immunoprecipitation in HA-tagged cyclin D1 overexpressed U2OS cells (experiments were done in triplicates). OE: overexpressed; sg: single guide; NT: non-target; EV: empty vector; ns: not significant. CRISPRi: CRISPR interference; KD: knock-down; WT: wild-type. Error bars represent SEM.

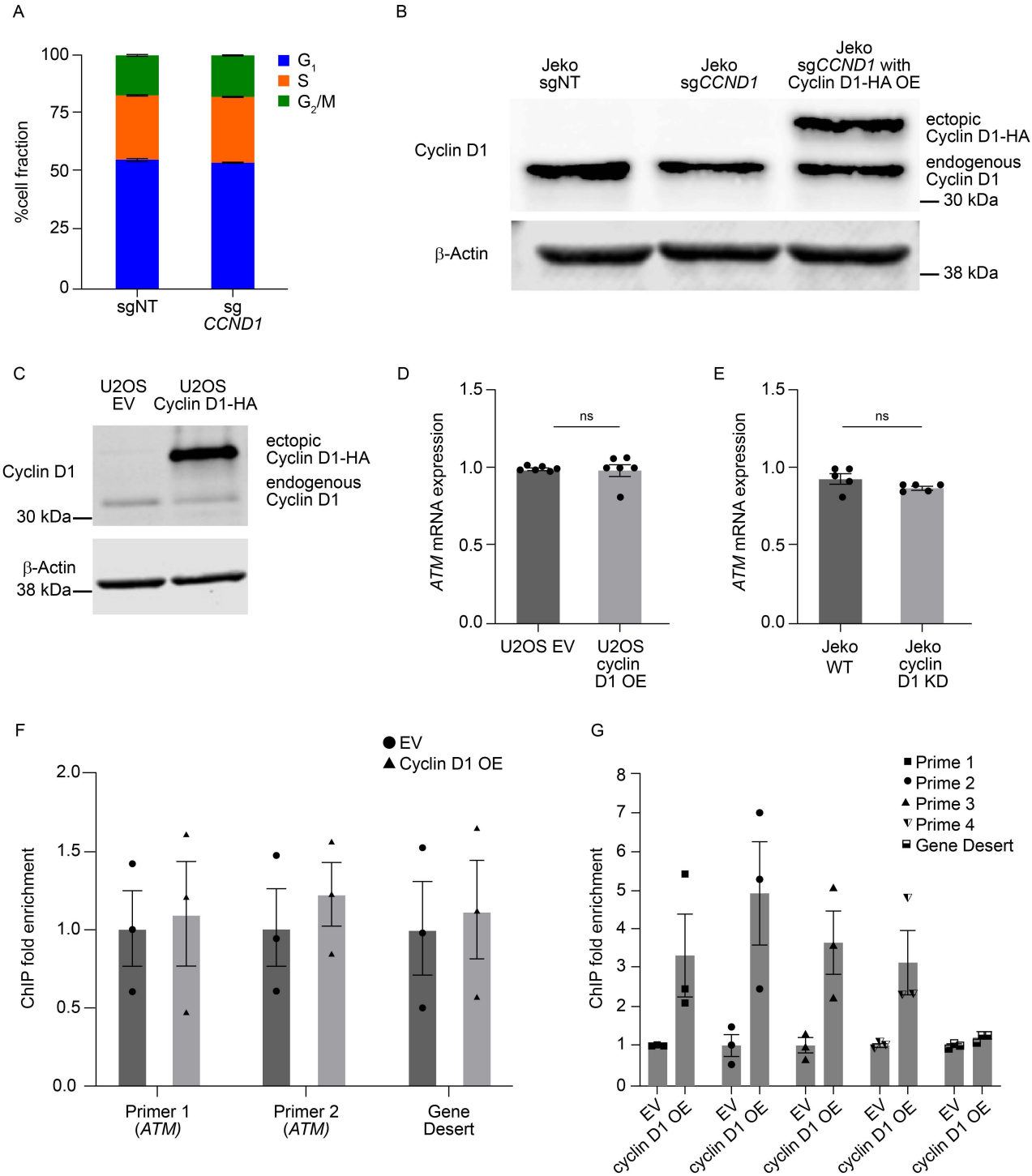

Supplemental Figure 3

Supplemental Figure 4: (A-C) Immunoblot depicting cyclin D1 overexpression and ATM deficiency in reporter cells used to assess DNA double-strand break repair pathways (Figure 4E and Supplemental Figure 4, I and J). **(D)** Immunoblot assessment of ATM in isogeneic ATM deficient and proficient cells. **(E)** Assessment of *POLQ* expression in cyclin D1 overexpressing U2OS cells with and without ATM deficiency (experiments were done in triplicates, p value was calculated using t-test). **(F)** Assessment of *POLQ* expression in primary MCL cells (n=20 ATM proficient and n=7 ATM deficient patients)**. (G** and **H)** Assessment of *POLQ* (G) and CCND1 (H) expression in MCL primary cells with and without ATM mutation using publicly available gene expression dataset (ref 56, p-value was calculated using t-test). **(I** and **J)** Assessment of NHEJ (I) and HR (J) activity with cyclin D1 overexpression and ATM deficiency using standardized reporter assays (experiments were done in quadruplicates, p-value is calculated by one-way ANOVA with Tukey's post-hoc test). OE: overexpressed; KO: knock-out; MMEJ: microhomology mediated end-joining; HR: homologous recombination; NHEJ: non-homologous end-joining; EV: empty vector; wt: wild-type; mut: mutant; MCL: mantle cell lymphoma; ns: not significant; **p<0.01. Error bars represent SEM.

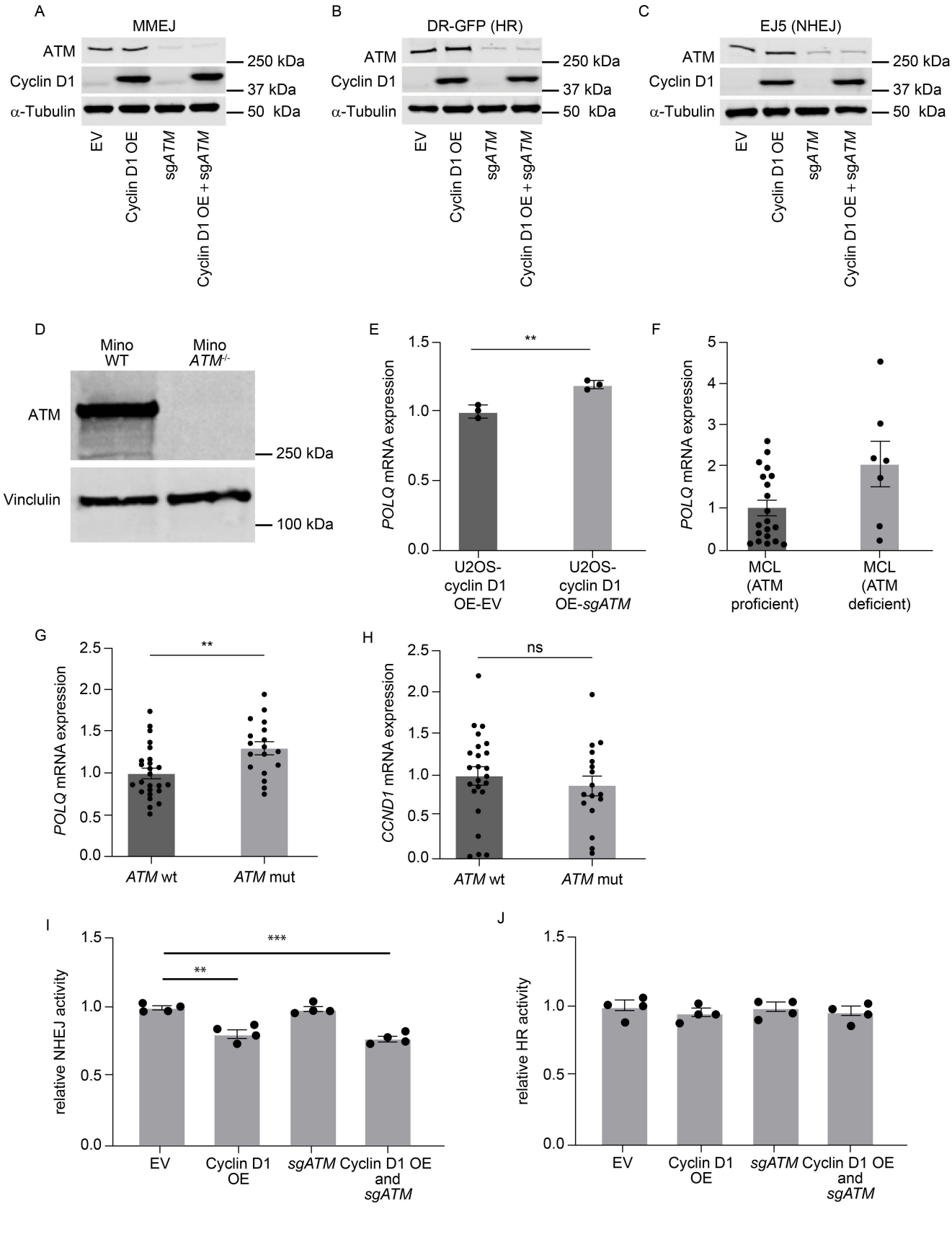

Supplemental Figure 4

Supplemental Figure 5: (A) Assessment of antiproliferative effect with *POLQ* depletion in multiple MCL cell lines (experiments were done in triplicates). **(B)** Probing for ATM pathway activity after radiation (2 Gy) in multiple MCL cell lines in which Granta, UPN2, and MCIR were identified as ATM-deficient (experiments were done in triplicates). **(C** and **D)** Assessment of sensitivity to POLΘ inhibition using ART558 (C) and NVB (D) in U2OS cells with respective genetic backgrounds (cyclin D1 overexpressed and ATM-deficient, experiments were done in triplicates). sg: single guide; NT: non target; OE: overexpressed; GFP: green fluorescent protein; NVB: novobiocin; Gy: Gray. Error bars represent standard deviation.

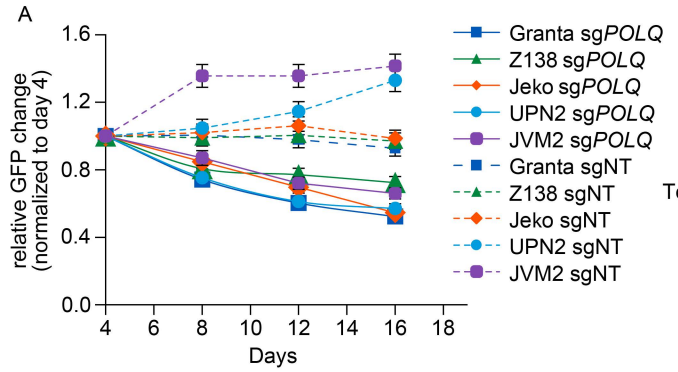

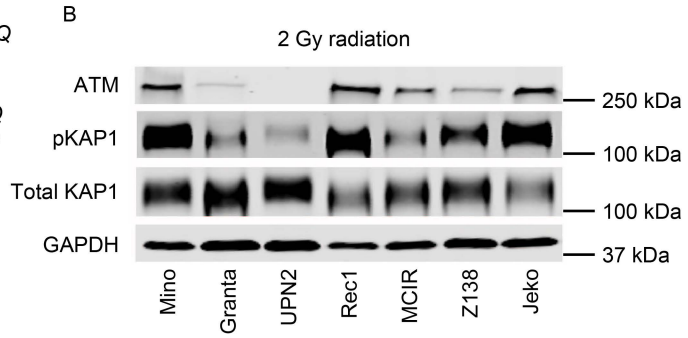

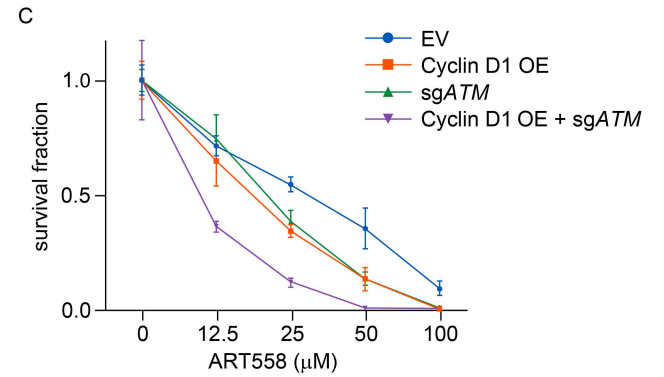

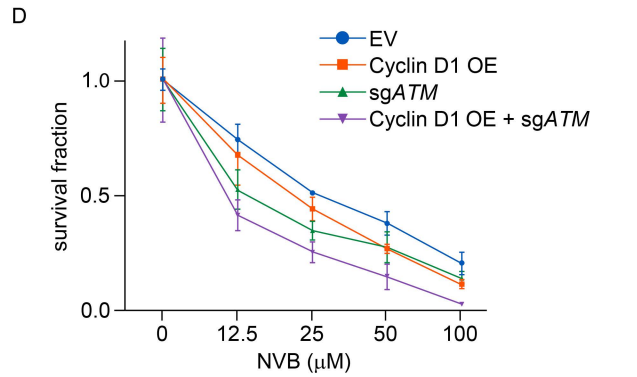

Supplemental Figure 5

Supplemental Figure 6: Measurement of body weight of mice bearing respective tumor types along the treatment period (eight mice per treatment group). PBS: phosphate buffered saline; NVB: novobiocin. Error bars represent SEM. Each data point represents the mean of body weights of all mice in each treatment group.

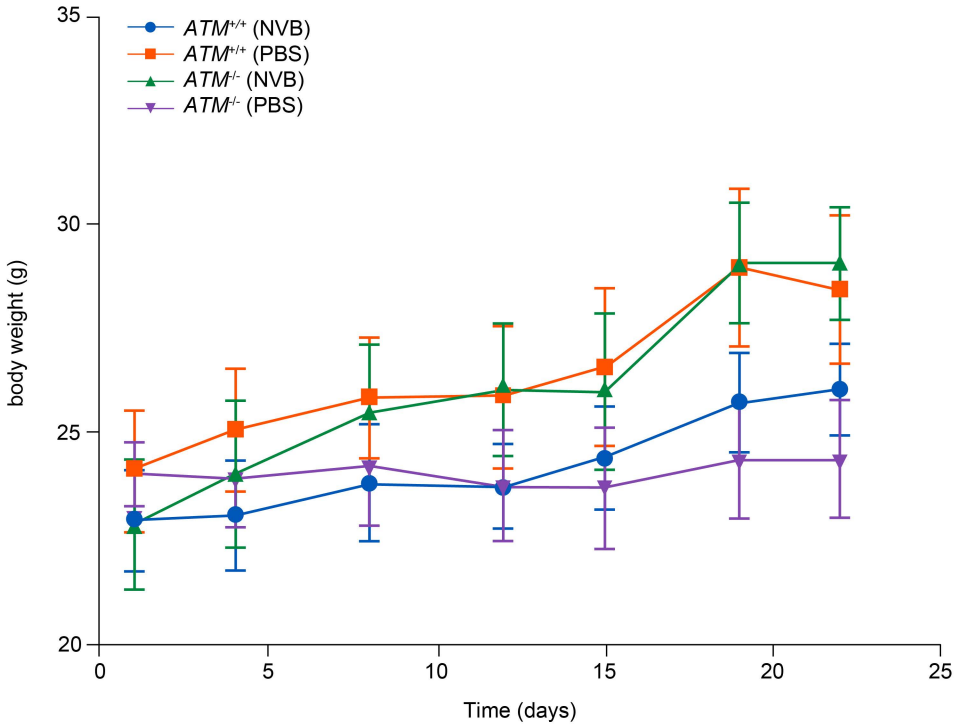

Supplemental Figure 6

Supplemental Figure 7: (A) Assessment of cyclin D1 in non Hodgkin lymphoma (MZL n=1, FL n=1, CLL n=1 and MCL n=5). **(B)** Assessment of ATM and cyclin D1 through immunoblotting in primary MCL patients (n=28). Squares represent patients with ATM deficiency. * Represent patients who were not included in the *POLQ* mRNA expression assessment in Figure 8B or cell viability assessment with POLΘ inhibition in Figure 8C due to low number of cells in the primary sample. MZL: Marginal zone lymphoma, FL: Follicular lymphoma, CLL: Chronic lymphocytic leukemia, MCL: Mantle cell lymphoma.

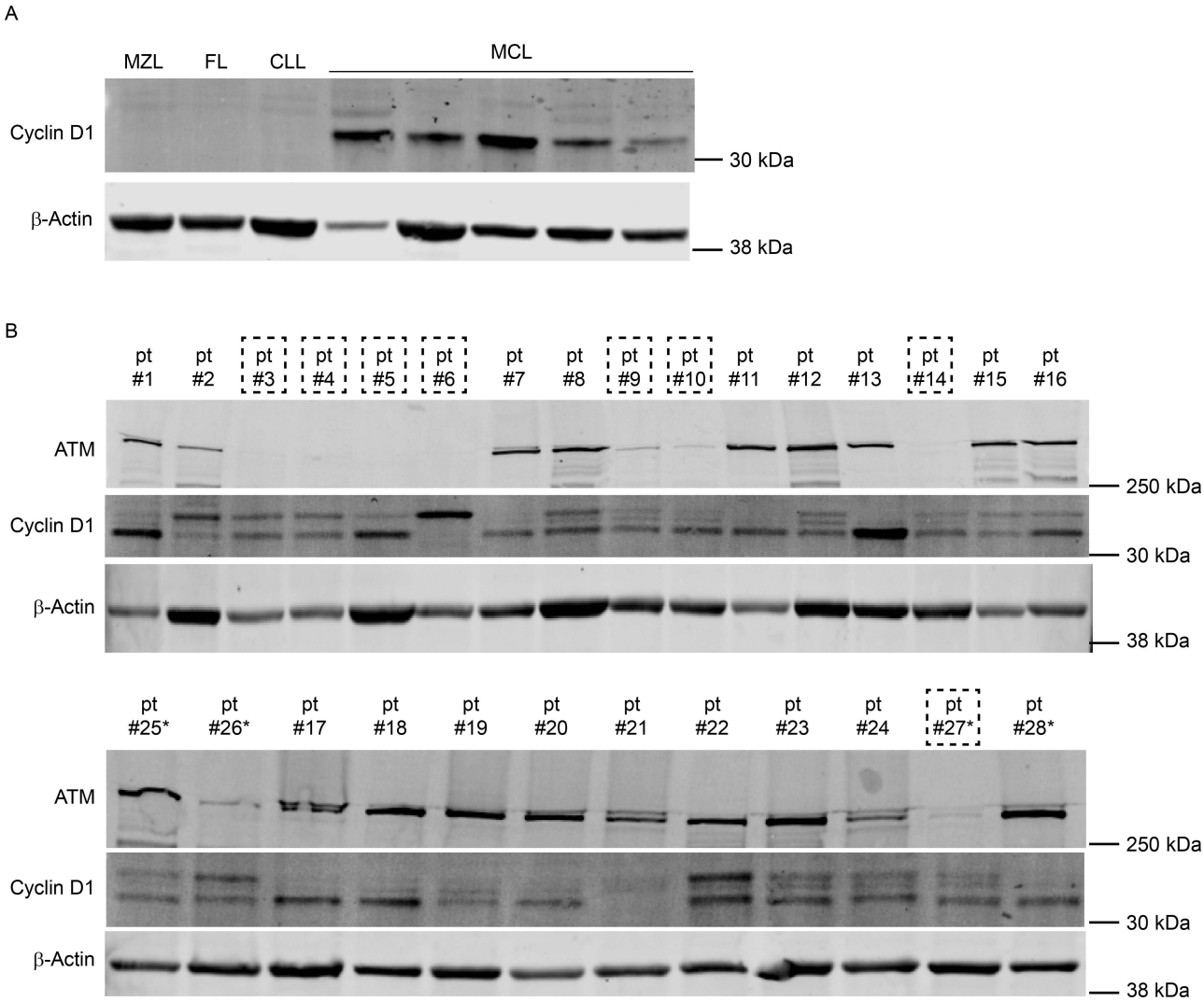

Supplemental Figure 7

Supplemental Table 1: Guide RNA used for CRISPR knock out, knock in and interference experiments

Gene Name	Guide RNA sequence
CRISPR KO	
POLQ (sgRNA)	1. TCTGATCAATCGCCTCATAG 2. CTGACTCCAAAAGCGGTACA 3. GCATGTACTAGAATGTAACA 4. TGCCCGGAAGGCAGTGGATG
ATM (sgRNA)	1. TTTAAGCATATCATAGACCT 2. ATATGTGTTACGATGCCTTA 3. CTTCTACCCCAACAGCGACA 4. TTATTCCAGAAAGCCAAGGT
NT (sgRNA)	1. CGCUUCCGCGGCCCGUUCAA
CRISPR KI	
POLQ (sgRNA)	1. TTGCCATGAATCTTCTGCGT
CRISPR interference	
CCND1 (sgRNA)	1. CACCGTGCCAACCTCCTCAACGACC 2. CACCGCATTTGAAGTAGGACACCGA 3. CACCGGAGCTGGTGTTCCATGGCTG 4. CACCGGCAGAAGCGAGAGCCGAGCG